

Journal Pre-proof

Portable XRF applied to regional bedrock mapping in Quebec, Canada

Pierre-Simon Ross, Mélanie Beaudette, Yannick Daoudene



PII: S0375-6742(24)00013-X

DOI: <https://doi.org/10.1016/j.gexplo.2024.107397>

Reference: GEXPLO 107397

To appear in: *Journal of Geochemical Exploration*

Received date: 19 August 2023

Revised date: 27 November 2023

Accepted date: 2 January 2024

Please cite this article as: P.-S. Ross, M. Beaudette and Y. Daoudene, Portable XRF applied to regional bedrock mapping in Quebec, Canada, *Journal of Geochemical Exploration* (2023), <https://doi.org/10.1016/j.gexplo.2024.107397>

This is a PDF file of an article that has undergone enhancements after acceptance, such as the addition of a cover page and metadata, and formatting for readability, but it is not yet the definitive version of record. This version will undergo additional copyediting, typesetting and review before it is published in its final form, but we are providing this version to give early visibility of the article. Please note that, during the production process, errors may be discovered which could affect the content, and all legal disclaimers that apply to the journal pertain.

© 2024 Published by Elsevier B.V.

Portable XRF applied to regional bedrock mapping in Quebec, Canada

Pierre-Simon Ross^{1,*}, Mélanie Beaudette², Yannick Daoudene²

1. Institut national de la recherche scientifique, 490 rue de la Couronne, Québec (Qc), G1K 9A9, Canada, pierre-simon.ross@inrs.ca

2. Ministère des Ressources naturelles et des Forêts du Québec, 5700, 4e Avenue Ouest, Québec (Qc), G1H 6R1, Canada, melanie.beaudette@mern.gouv.qc.ca
yannick.daoudene@mrnf.gouv.qc.ca

*Corresponding author

Abstract

Whole-rock geochemistry yields better geological maps of the bedrock, since it allows, for example, visually similar lithologies to be distinguished. However, conventional laboratory geochemistry is not available in the field during a mapping campaign. Portable X-ray fluorescence (pXRF) analyzers can produce fit-for-purpose data rapidly, and constitute a useful complement to conventional geochemistry in a bedrock mapping project. The pXRF data can be employed (i) while still in the field, to orient the mapping campaign; (ii) to prepare a preliminary geological map back in the office; and (iii) to interpolate between conventional whole-rock analyses on the final map. The latter application requires a matrix-matched secondary calibration of the pXRF data to improve its accuracy. Attention must also be given to precision issues, as well as potential instrument drift and analytical interferences.

This paper summarizes recent efforts to systematically integrate quantitative pXRF data in government mapping projects within the Province of Quebec (Canada). We first demonstrate how an Olympus Vanta series M pXRF analyzer was commissioned and calibrated. We then show how the pXRF data was systematically acquired and utilized during a 1:50 000 to 1:20 000 mapping campaign in a Precambrian greenstone belt setting (Abitibi Subprovince). Before the mapping began in 2021, volcanic rocks in the study area were supposed to consist of only two mafic tholeiitic formations, called Obatogamau and Bruneau. Integrating pXRF into this project meant that while still in the

field and immediately afterwards during preparation of the preliminary map: (1) a marker horizon representing the top of the Obatogamau Formation was chemically identified and then traced laterally; (2) the felsic Waconichi Formation was recognized despite the high metamorphic grade and also traced laterally just above the marker horizon; (3) the Bruneau Formation was shown to be much more continuous than previously known and to have Mg-tholeiites at its base, like in the type locality; (4) the Blondeau Formation was shown to occur above the Bruneau Formation. Within the volumetrically dominant Obatogamau Formation, Fe-tholeiites were also distinguished from visually similar Mg-tholeiites, which allowed these subunits to be traced while still in the field, leading to a more detailed map. Later, after the conventional laboratory chemistry had been received, the final geological map was prepared, but it was very similar to the preliminary map, confirming the satisfactory performance of the pXRF method for this application. However, we do note some issues and limitations even with the latest generation of analyzers.

Keywords

Geological mapping; portable X-ray Fluorescence analyzers; lithological discrimination; accuracy; precision; calibration

1. Introduction

When mapping the bedrock at scales such as 1:20 000 or 1:50 000, whole-rock geochemistry can be very useful to separate visually similar lithologies into groups. When the geochemical groups are regionally mappable, this produces a more detailed map than relying only the visual aspect of the rock. For example, in a Precambrian greenstone belt setting, a single map unit of mafic lavas occupying half a map sheet or more may be subdivided into several geochemical groups. This can result in a better stratigraphic understanding and may help to unravel the structural history of the region. Different types of fine-grained intrusions or different varieties of fine-grained sedimentary rocks could also be potentially distinguished based on geochemical or petrographic characteristics. Unfortunately, geochemical results from conventional laboratory techniques (e.g., WD-XRF, ICP-AES, ICP-MS) are typically not available

during the field campaign, and may not even arrive in time to produce a preliminary geological map during the first few months back in the office.

This is where portable X-ray fluorescence (pXRF) analyzers can play an important role, since that type of geochemical data, although less precise and less accurate, can be made available within a few days of collecting the sample. The pXRF data can then be used (i) while still in the field, to orient the rest of the mapping campaign; (ii) to compile a preliminary geological map; and (iii) to interpolate between conventional geochemical analyses on the final version of the map (Ross and Beaudette, 2021). The samples collected for pXRF measurements can also be employed to measure physical parameters such as density and magnetic susceptibility, and photographed under controlled lighting conditions, to maximize the information gathered on each sample, in a “field laboratory” type of installation (Fig. 1a).

However, obtaining *in situ* pXRF data that is precise enough to be useful in lithological discrimination, and accurate enough to be plotted alongside conventional geochemistry, is not a trivial undertaking. When purchasing and commissioning a new pXRF analyzer, producing quantitative data is not a “point-and-shoot” exercise. First, there must be a QA/QC program that includes blanks and reference materials (e.g., Fisher et al., 2014; Le Vaillant et al., 2014; Zhang et al., 2017; Lemière, 2018). Then, before quantitative analyses can be made, the user must determine the optimal measurement time and number of spots per sample, and establish a matrix-matched secondary calibration (Hall et al., 2013, 2014; Le Vaillant et al., 2014; Ross et al., 2014a, 2014b; Bourke and Ross, 2016; McNulty et al., 2018; Martin and Carr, 2020; Adams et al., 2021). The analyzer can then be taken in the field – or more specifically in a field laboratory – to provide quantitative data for some elements. But ultimately the secondary calibration must be validated based on a larger dataset, i.e. conventional laboratory geochemistry must be compared with corrected pXRF data on a subset of the unknown samples (Le Vaillant et al., 2014; McNulty et al., 2018; Ahmed et al., 2020; Ross and Beaudette, 2021).

In this paper, we summarize the recent work done on acquiring pXRF data on igneous rocks with an Olympus Vanta analyzer and applying that to regional geological mapping of Precambrian greenstone belts at *Ministère des Ressources naturelles et des Forêts du Québec* (MRNFQ), in collaboration with *Institut national de la recherche scientifique* (INRS). We show that pXRF data is useful at all stages of a bedrock mapping project: (i) while still in the field, to get an idea of the composition and magmatic affinity of the rocks, separate the volcanic rocks into geochemical groups, and orient the field work; (ii) for the preliminary map, to refine the volcanic stratigraphy, and (iii) for the final map, to interpolate between conventional whole-rock analyses. In our opinion, these results easily justify the additional work involved in acquiring pXRF data during a bedrock mapping campaign. We do note, however, that for some chemical elements there are remaining issues with poor precision, poor accuracy, instrument drift, or analytical interferences.

2. Materials and methods

2.1 Analytical equipment and sample preparation

The pXRF analyses presented here were made with an Olympus Vanta analyzer, series M (serial number 807198). Such devices are equipped with 50 kV X-ray tubes and large-area silicon drift detectors (Olympus, 2021). All measurements were made within a Vanta Workstation, which is a hands-off closed-beam setup (Fig. 1b). The instrument was controlled by a laptop computer.

The specific analyzer we used offers two analytical modes, Geochem and Soil. The (3-beam) Geochem mode is based on fundamental parameters (Frahm, 2017; Olympus, 2021) and attempts to measure to as many elements as possible; this was formerly called the “Mining” or “Mining Plus” mode by Olympus, for example in the Delta analyzers. The Soil mode relies on Compton normalization and mostly targets trace elements (see Hall et al., 2013, for a more detailed description of these analytical modes). Both modes feature three ‘beams’, which are optimized for different elements based on different X-ray tube voltages and the metallic filters being used (Frahm, 2017; Bezur et al., 2020). The user can control beam time. Many elements are available in both modes, so users must empirically choose which mode is best for each of those elements in their samples.

All pXRF measurements presented here were made *in situ* on flat rock surfaces, either cubes or slabs ≥ 1 cm-thick, of dense (very low porosity) Precambrian rocks. The flat surfaces were obtained by cutting the samples with a diamond blade, washing them with water, and letting them dry overnight. Flat weathering-free surfaces are important to avoid the effects of chemical weathering and surface relief (irregularities), which can lead to higher or lower average values of some elements, as well as more dispersed (scattered) results (Potts et al., 1997, 2006; Lundblad et al., 2011). Dry analytical conditions are important because water attenuates X-rays (Ge et al., 2005).

In typical *in situ* pXRF work on volcanic and intrusive rock samples, it has become common practice to average several measurement spots for each sample, to account for mineralogical heterogeneity (e.g., Bourke and Ross, 2016; McNulty et al., 2018, 2020; Ahmed et al., 2020; Jimenez-Gonzalez, 2020; Adams et al., 2021; Wells et al., 2021). To facilitate shifting the sample by a fixed distance between each analytical spot, a grid with a spacing of 12 mm was placed at the bottom of the workstation (Fig. 1c). This insures that there is no overlap between spots, yet that as many spots as possible can be analyzed, if needed.

2.2 Overview of datasets

This paper uses two pXRF datasets. The commissioning dataset was acquired in 2020-21 before the mapping campaign started, using 20 archived rock samples (Beaudette et al., 2021). The Vanta analyzer, which was new at the time, was tested to optimize beam time and the number of spots per sample, and to establish analyzer-specific matrix-matched secondary calibration lines. This commissioning dataset is accompanied by conventional laboratory geochemistry on the same 20 samples.

The bedrock mapping dataset consists of pXRF analyses of 374 unknown samples made within a field laboratory setting during a 2.5 month-long geological mapping campaign in summer 2021. The analytical protocol and the secondary calibrations for these measurements were chosen based on evaluation of the commissioning dataset. This

bedrock mapping dataset is accompanied by conventional laboratory geochemistry on a subset of the same samples, for validation purposes.

2.3 Commissioning dataset

We rely on the commissioning dataset to establish a secondary calibration for the pXRF analyzer, as well as to optimize beam time and the number of spots to be averaged for each sample. Some previous authors have used certified reference materials in powdered form for the secondary calibration, but this can be problematic for *in situ* work on rocks. The reason is that for a number of elements, the pXRF response can be quite different for powders versus *in situ* analyses of the same geological materials. An extreme example is Al_2O_3 , for which in a previous study, Bourke and Ross (2016) compared the pXRF averages versus traditional geochemistry for a range of rock samples and obtained a linear regression slope of 0.9 for *in situ* pXRF analyses but 0.3 for uncompact powders covered by a plastic film (see their Fig. 5). There are no certified reference materials in unprepared rock form that we could use instead of powders. So over the last decade, we have been using rock samples similar in composition and grain size to those that we want to routinely study to calibrate pXRF analyzers for *in situ* work on rocks (Ross et al., 2014a; Bourke and Ross, 2016; Ross, 2019). The idea is to select a representative suite of samples, perform a large number of *in situ* pXRF analyses on each, and then send them out for conventional geochemistry.

In this study, for the commissioning dataset, 20 samples of dense Precambrian volcanic and fine-grained intrusive rocks were obtained from the archives of INRS and MRNFQ. They consist of 18 hand samples and two drill core samples. They come from the Abitibi Subprovince (Superior Province) and the Northern Domain of the Ungava Orogen (Churchill Province; Beaudette et al., 2020), both in Québec. The samples range in composition from komatiite to rhyolite, and in magmatic affinity from tholeiitic to calc-alkaline, covering the complete range of subalkaline volcanic rocks typical of the Precambrian bedrock in Canada (Tables 1 and 2). These samples were cut into slabs 1-2 cm-thick to obtain numerous smooth surfaces for pXRF measurements.

In each analytical mode (Geochem and Soil), on each of the 20 samples, 30 different spots were analyzed once, with a beam time of 20 s per beam, to evaluate accuracy and establish a secondary calibration. The idea was to cover the sample surface as much as possible to minimize the effect of mineralogical heterogeneity. The pXRF data was averaged for each mode and each sample. These pXRF averages were then plotted, for each element, against conventional laboratory geochemistry on the same samples. The latter was obtained from Agat Laboratories in Mississauga, Ontario (Canada) and relies on (i) lithium borate fusion followed by XRF for major oxides; (ii) sodium peroxide fusion followed by ICP-OES for Cr, Cu, Ni, S, Sr, V, Zn or by ICP-MS for As, Co, Nb, Rb, Y, Zr (Tables 1 and 2). Other elements and loss on ignition were also measured in this laboratory but are not used here. Certified reference materials employed by this laboratory include REE-1 (rare earth ore), SY-4 (syenite) and Till-2 (till sample) from Natural Resources Canada, as well as CGL-015 (syenite) from the Central Geological Laboratory of Mongolia. For Nb, the reported detection limit of 1 ppm was a little high for our purposes, with two samples of our 20 below the LOD and six more at or below the limit of quantification, LOQ (taken as three times the LOD). Therefore, we later (after the summer 2021 field season) had this element reanalyzed by another laboratory, Activation Laboratories (Ancaster, Ontario), by the same method, but with a detection limit of 0.2 ppm, which gave data above the LOD for the 20 samples, including only one sample below the LOQ. The certified reference materials employed by this lab for Nb include BIR-1a (basalt) from the USGS, SARM 3 (lujaurite) from the South Africa Bureau of Standards, and USZ 42 2006 (rare earth ore) from the Central Geological Laboratory of Mongolia.

These graphs of pXRF average against conventional laboratory geochemistry allowed a secondary calibration to be established using a linear regression, when the pXRF data was deemed robust, i.e. highly correlated to the conventional geochemistry. For simplicity, we show the least squares regressions with pXRF as the x axis since this gives the correction directly, although this incorrectly assumes that pXRF data are error-free. We also evaluated a type of regression that takes errors on both axes into account, functional relationship estimation by maximum likelihood (FREML; Ripley and

Thompson, 1987; Analytical Methods Committee, 2002) and this yielded very similar results for most elements, so we only show the least-squares regressions here. The same graphs also allowed us to decide which mode, Geochem or Soil, performed better, for each element. Criteria used for that decision were accuracy based on factory calibration (linear regression slope closest to 1.0, intercept closest to zero); the dispersion of data points (R^2 closest to 1.0); and the most samples out of 20 returning values above the detection limit by pXRF. Some elements were not deemed robust by pXRF, i.e. they were detected in only a few samples, and/or the correlation was weak with conventional laboratory geochemistry.

Three of the 20 calibration samples were also utilized to optimize beam time and the number of spots, in both analytical modes. Sample precision is the relative standard deviation (RSD) of a series of measurements on different spots on the rock surface (Le Vaillant et al., 2014; Bourke and Ross, 2016). Previous studies using *in situ* pXRF on volcanic and fine-grained intrusive rocks have shown that the variability of measurements on different spots, due mostly to mineralogical heterogeneity, is much greater than the variability on single spots, due to random analytical errors (Le Vaillant et al., 2014; Bourke and Ross, 2016). In other words, sample precision – not analytical precision – is the parameter to optimize to get representative pXRF measurements (Ross, 2019). Optimizing sample precision requires varying both the beam time and the number of spots to find a suitable combination. For this exercise, we employed samples ranging in composition from komatiite to rhyolite and in texture from relatively uniform to strongly porphyritic, to obtain best-case and worst-case results for each element of interest. These three samples are:

- 19-GL-2141-A, a pyroxene- and plagioclase-phyric komatiitic basalt, with 15-20% phenocrysts in a much finer groundmass (Fig. 1d);
- “Spinifex Ridge”, a komatiite lava sample with a random olivine spinifex texture (Fig. 1e);
- 2012-JG-9245-A, a rhyolite with 10% feldspar and quartz phenocrysts, 2-4 mm across, in a very fine groundmass, as well as 5% amygdales and 1% disseminated pyrite (Fig. 1f).

For each of these three samples, 30 spots were measured once for each predetermined beam time. These beam times were 12, 15, 18 and 20 s for 19-GL-2141-A, and 5, 10, 15, 20 s for the other two samples. In the literature, longer beam times (30 s or more) are commonly employed, especially for powdered samples which can be measured only once or twice in one spot since they are already homogenized (e.g., Fisher et al., 2014; Le Vaillant et al., 2014; Piercey and Devine, 2014). However, recall that (i) the Vanta series M is a significantly faster pXRF device than those of the previous generation used in most previous studies; (ii) we are measuring multiple spots *in situ* on rock slabs, and mineralogical heterogeneity is an important issue that is not addressed by longer beam times; (iii) we are trying to optimize sample precision, not analytical precision. Of the 30 spots obtained, we calculated moving averages for 1, 2, 5, 7 and 9 spots, for each element and each sample. We then computed RSDs from these moving averages.

2.4 Bedrock mapping dataset

The study area is located in the NE corner of the Abitibi Subprovince in Quebec, about one hour drive west of the town of Capois. The Archean bedrock geology of a portion of topographic sheets NTS 32G13 and 32J04 was mapped by MRNFQ at a scale between 1:20 000 to 1:50 000 during summer 2021 (Daoudene and Beaudette, 2021). Archean volcanic rocks, which were the focus of pXRF efforts, belong to the Roy Group (e.g., Daigneault and Allard, 1999; Leclerc et al., 2011). For the purpose of pXRF measurements, an attempt was made to collect a 1-2 kg representative sample from all outcrops containing:

- volcanic rocks;
- intrusive rocks with a fine-grained (<1 mm) to medium-grained (1-5 mm) texture, but excluding those with a coarse to pegmatitic grain size;
- sedimentary rocks from mudstone to sandstone (but excluding conglomerate).

The samples were brought back to town, then cut into cubes or similar shapes to eliminate weathering rinds and obtain flat smooth surfaces. Within a field laboratory setting, photographs were taken of each sample, as well as measurements of the density, magnetic susceptibility, and chemical composition with pXRF (Fig. 1).

For the pXRF measurements, based on results from the commissioning dataset which will be presented below, it was decided to employ both analytical modes (Geochem and Soil), 9 spots per sample, and 10 s per beam, for the bedrock mapping campaign. This involved about 10 minutes of pXRF measurements per sample, excluding sample preparation. Over the summer, 374 samples were thus analyzed by pXRF, including 184 volcanic samples, 132 intrusive samples, 49 sedimentary samples, and 9 “other” samples (migmatites, mylonites).

Of those, 82 volcanic samples, 78 intrusive samples, and 17 sedimentary samples were also analyzed by conventional laboratory geochemistry at Activation Laboratories, using code 4LithoRes. This implies fusion ICP-AES for major oxides and some trace elements (Co, Pb, Sr, V, Zr), fusion ICP-MS for Nb, Rb, Y and trace acid ICP-AES for Cu, Ni, Zn. (The 4LithoRes package also includes several other elements not readily obtained by pXRF and not discussed here.) We use this independent conventional whole-rock geochemical dataset to validate our secondary calibrations and detect any analytical interference issues in the pXRF data.

3. Results

3.1 Commissioning dataset

3.1.1 Sample precision

Obtaining a sample precision – expressed as the RSD of a series of spots on the sample – of 5% or less would be desirable, but is difficult to achieve for some elements in some samples. In this study, we took 10% RSD as our general target. What is the required combination of beam time and number of spots needed to achieve that?

On plots of RSD versus beam time (Figs. 2-5), for the beam times and three materials investigated, the vast majority of the curves are flat, i.e. there is no noticeable gain in sample precision with longer beam times. On the other hand, vast improvements in RSD are available by averaging three to five spots per sample, compared with measuring only a single spot. Improvements in RSD continue at lesser rates up to seven spots for most

elements, and up to nine spots for some elements in some samples, for example Zr in the komatiite (Fig. 4f). Taking all of the elements into account in the three tested samples, in both analytical modes, we propose that averaging nine spots per sample but using only 10 s per beam is a good compromise between total measurement time and sample precision, for *in situ* work on slabs of volcanic rocks, using the Vanta series M devices.

In Geochem mode, based on the 10-12 s beam times and 9 spots, we expect sample precision to be better than 5% in *most* samples for Al_2O_3 , Fe_2O_3^t , MnO, SiO_2 , Sr, Y, Zn, and Zr, and better than 10% in *most* samples for CaO and P_2O_5 . The typical RSDs are less clear for MgO: the performance is good for ultramafic to mafic rocks (Figs. 2c, 4c), but needs to be investigated for intermediate and felsic rocks, closer to the detection limit. For V, the RSD behavior is somewhat chaotic in the current dataset.

In Soil mode, based on the same settings (10-12 s beam times and 9 spots per sample), we expect sample precisions better than 5% in *most* samples for TiO_2 , and better than 10% in *most* samples for Cr, Nb, and Ni. In that same mode, RSDs will likely be higher than 10% for Cu and Rb in unmineralized or relatively low-Rb samples. The RSDs for K_2O seem highly concentration-dependent, but can be lower than 5% in felsic samples.

The RSDs reported the previous two paragraphs are for the elements based on their 'best' analytical mode, as established in the next section. The other elements programmed in the analyzer but not mentioned above do not exhibit a robust performance in the commissioning dataset.

For a given beam time and number of spots, sample precision depends on both elemental concentration and sample texture. We focus on the RSDs for 10 s or 12 s beam times but the nine point moving averages, in Geochem mode, to illustrate our point. One example where the effect of elemental concentration dominates is CaO: the sample with the highest concentration (the komatiitic basalt, with about 12% CaO) has the lowest RSD, under 2%, and the sample with the lowest concentration (the rhyolite, with about 2% CaO) has the highest RSD, about 10% (Figs. 2b, 4b, 5b).

In contrast, the effect of rock texture seems dominant for Sr. Both the komatiitic basalt and the rhyolite have Sr contents in the 110-120 ppm range, yet the RSD is about 5% for the former and about 2% for the latter. We interpret this difference as related to the strongly porphyritic texture (with abundant coarse phenocrysts, including plagioclase) of the komatiitic basalt. The komatiite has an intermediate RSD between the other two, despite having a much lower Sr concentration (31 ppm) (Figs. 2d, 4d, 5d).

3.1.2 Secondary calibration and best mode for each element

The secondary calibration exercise shows that for our unmineralized Precambrian bedrock samples of volcanic to intrusive origin, based on *in situ* work on slabs, the following 19 elements are robust in at least one of the analytical modes: the major oxides Al_2O_3 , CaO , $\text{Fe}_2\text{O}_3^{\text{T}}$, K_2O , MgO , MnO , P_2O_5 , SiO_2 , and TiO_2 and the trace elements Cr, Cu, Nb, Ni, Rb, Sr, V, Y, Zn and Zr. This means that (i) most of the 20 samples considered for this exercise produced results above the detection limit and that (ii) these elements don't need much of a secondary calibration, or that a systematic error exists, but can be corrected to fit with the conventional geochemistry, using the linear regressions on the graphs of conventional laboratory geochemistry versus uncorrected pXRF (Figs. 6-7, Table 3).

The performance of the Geochem mode is notable, and using it alone would have been acceptable for most of the 19 elements listed above. However, based in part on the number of samples above the detection limit in the commissioning dataset, the Soil mode is clearly superior for Cr, K_2O , Nb and Rb (Table 3). For example, in the case of Nb, only nine samples out of 20 could be analyzed in Geochem mode (Fig. 8c), but 17-20 could in Soil mode (Fig. 7d), indicating better detection limits. Since Nb is included on the Winchester and Floyd (1977) diagram for classifying volcanic rocks, and since K_2O is useful in hydrothermal alteration studies, our assessment is that combining both modes is worth it, despite the additional time investment of adding the Soil mode. Therefore, based on all the criteria listed in section 2.3, we prefer the Geochem mode for Al_2O_3 , CaO ,

Fe_2O_3^T , MgO, MnO, P_2O_5 , SiO_2 , Sr, V, Y, Zn and Zr, whereas we prefer the Soil mode for K_2O , TiO_2 , Cr, Cu, Nb, Ni, and Rb (Table 3).

The secondary calibration exercise also shows that some elements can't reliably be measured by pXRF in our samples. This includes As and Co (Figs. 8d, 8e) as well as Ag, Ba, Bi, Cd, Hg, Mo, Pb, S, Sb, Se, Sn, Ta, Th, U, W, and the rare earth elements (not shown). Problems include (i) few, if any, samples yielded values by pXRF, indicating elevated detection limits, relative to concentrations in samples from the commissioning dataset, (ii) lack of correlation with conventional geochemistry, (iii) analytical interferences.

3.2 Bedrock mapping dataset

3.2.1 Use of pXRF data during field work

In this project, the pXRF data (bedrock mapping dataset) was used in the field to get an idea of the composition and magmatic affinity of volcanic rocks as the mapping progressed. Two thirds through the campaign, it was already clear, based on consistent southward younging indicators, that the volcanic succession was a homoclinal one, which facilitated the stratigraphic understanding of this succession. At this stage, a very preliminary geological map was compiled during a single day, using geophysical surveys, lithological and structural observations, and pXRF data. This exercise allowed preliminary geochemical groupings to be established within the volcanic rocks, and recognition that a marker horizon with a transitional affinity existed at the top of the Obatogamau Formation. Further field work during the last third of the mapping campaign targeted this contact. Immediately above the marker horizon, a metamorphosed garnet-bearing unit was recognized as felsic and calc-alkaline based on pXRF and this led to the idea that this horizon represented the Waconichi Formation, at the top the first cycle of the Roy Group. The Waconichi Formation has historically been the main target of exploration for volcanogenic massive sulfide deposits in the Chapais-Chibougamau area further east (e.g., Leclerc et al., 2011; Ross et al., 2016). That assignment, plus recognition of a Mg-rich tholeiitic unit just above the Waconichi Formation – similar to the situation in the Chibougamau area (Leclerc et al., 2011) – meant that the volcanic

rocks just above the Waconichi Formation could be assigned to the Bruneau Formation, which was not previously known to be widespread in this area. The rocks just above the Bruneau Formation were therefore called 'Blondeau Formation' based on volcanic textures and their calc-alkaline signature. The Blondeau Formation was not known from the study area previously. Another use of the pXRF data in the field was to help target Zr-rich samples for U-Pb dating on zircons. Those U-Pb ages are not yet available.

3.2.2 Use of pXRF data to compile a preliminary map

A much more detailed preliminary map was compiled a few weeks after the end of the field season (Daoudene and Beaudette, 2021). This map was based on all information available at the time, which included pXRF (bedrock mapping, dataset) but not conventional laboratory geochemistry. A simplified version of the volcanic portion of this 1:50 000 to 1:20 000 map is presented in Fig. 9. Highlights include:

- The mafic to intermediate volcanic rocks from the Roy Group are assigned to four different formations, from stratigraphic top to bottom: Blondeau, Bruneau, Waconichi, Obatogamau. This assignment is based mostly on lithology, stratigraphic position (Fig. 9) and pXRF data (Fig. 10).
- Lavas from the Obatogamau Formation are separated into three units based on pXRF: Fe-tholeiite, Mg-tholeiite, basalt of transitional affinity (Fig. 10)
- The Bruneau Formation is separated into two visually similar units based on pXRF: Fe-tholeiite and Mg-tholeiite (Fig. 10)

In short, without pXRF information, the mafic volcanic rocks of the Bruneau and Obatogamau formations would have each been one undifferentiated green unit on the map; separating them into several units shows the trends in the lava stratification and yields a more detailed, more useful map.

3.2.3 Use of pXRF data in the final geological map

The final geological map for the project, produced some months later (Daoudene and Beaudette, 2022), incorporated the conventional laboratory geochemistry and petrographic information as well as the pXRF data (Fig. 11). That final map is very similar to the preliminary map, showing the fit-for-purpose character of the pXRF data

for regional geological mapping projects. The conventional geochemistry validated the geological contacts, the geochemical groupings, the rock names and the magmatic affinities. The only change was that the marker unit at the top of the Obatogamau Formation plots as calc-alkaline on the Ross and Bédard (2009) diagram (not shown), whereas on the Barrett and MacLean (1999) diagram it is transitional (Fig. 10c). The conventional data also allowed a complete geochemical characterization of the volcanic rocks, including extended trace element diagrams (spidergrams).

3.2.4 Validating the secondary calibration

The bedrock mapping dataset can also be used to check the “real life” performance of the secondary calibration and more generally, the performance of the pXRF analyzer on chemical elements relevant for mapping purposes. Although a quick version of this exercise was done when the final geological map was being produced in 2021-22, due to time constraints the detailed investigation presented here was only done afterwards, subsequent to Nb being reanalyzed in a second laboratory. In the future, the validation of pXRF results should be done as soon as conventional geochemical data becomes available.

We first evaluated whether instrumental drift could be an issue, using measurements done on a powdered reference material (NIST2711a) every day the analyzer was employed. Drift could have occurred between the calibration period (August-September 2020) and the bedrock mapping project (June-August 2021), and within latter period. We focus on the drift between 2020 and the average of the 2021 campaign. Drift was found to be negligible (typically within -1% and +1% relative) for the following oxides and elements: CaO, MnO, Fe_2O_3^T , Sr, Y, Zr in Geochem mode; K_2O , Rb in Soil mode. A noticeable amount of drift was observed for Al_2O_3 in Geochem mode (-0.3 wt. % absolute, or -3% relative) and for TiO_2 in Soil mode (+0.01 wt. % absolute, or +3% relative). Finally, significant drift was documented for SiO_2 (-2.8 wt. % absolute, or -5% relative) and P_2O_5 (-0.03 wt % absolute, or -13% relative) in Geochem mode, and for Nb in Soil mode (+1.5 ppm absolute, +9% relative). We did not use the P_2O_5 data in this study. For SiO_2 , average drift was added back to the raw data before applying the secondary calibration in

figure 12d, but not in figure 10a, which shows the data as it was used to produce the preliminary map. For Nb, there are also other issues to deal with, as discussed below. Drift was not taken into account for other elements.

Figures 12 and 13 show the conventional geochemistry versus the corrected pXRF data from the bedrock mapping dataset, with a few outliers excluded in some cases. The slope of the regression is close to one and the intercept close enough to zero for Fe_2O_3^T , MgO , SiO_2 and Y in Geochem mode and for K_2O , TiO_2 and Rb in Soil mode, showing a satisfactory performance. In several cases, this good performance was found despite having employed some of the secondary calibrations beyond their intended ranges due to the presence, for example, of trace element-rich felsic intrusives in the bedrock mapping dataset but not in the commissioning (calibration) dataset. For these elements and oxides, the corrected pXRF data and the conventional whole-rock data can be plotted together to classify rocks and help with geological mapping and this validates the use of the pXRF for this application.

However, slopes far from 1.0 (and intercepts far from zero for two elements) were found for Al_2O_3 and Y in Geochem mode and for Nb in Soil mode. For Al_2O_3 , most of the bedrock mapping dataset forms a cluster in a limited range, rather than being distributed from low to high values which would have helped with the regression; the cluster plots on the 1:1 line, but a regression through the data has a slope of only 0.66, with a low coefficient of determination (R^2). We interpret these results as a high dispersion, uncertain accuracy, but suggest that Al_2O_3 data is still usable (Fig. 12a). In the case of Y, R^2 is relatively high, and the 0.82 slope represents a bias that was not addressed by the secondary calibration (Fig. 12e). The cause of this bias is not understood, as it is neither due to instrument drift nor analytical interference from Rb (cf. Conrey et al., 2014; Wilke et al., 2016). Nevertheless, the Y data is still close enough to the 1:1 line to use it, given the major differences in Zr/Y ratios between different geological units (Fig. 10c). Finally, the poor performance for Nb is disappointing as this element is used in a classification diagram (Fig. 10b). Using the secondary calibration based on the Actlabs data (the second laboratory), rather than that of Agat laboratory (the initial laboratory), helps with the

slope but not with the intercept, which remains at -3 to -4 ppm; the corrected data plots well away from the 1:1 line, unlike for all other elements shown (Figs. 13c, 13d). This poor performance for Nb seems to be caused by numerous basalts in the bedrock mapping dataset having Nb concentrations not far from the detection limit (creating scatter), to a limited extent by instrument drift (not corrected for, given other problems) and to a large extent by analytical interferences with Y, as previously documented by Conrey et al. (2014) and Wilke et al. (2016) for a different analyzer. Figure 13e shows a correlation between the Nb overestimation by pXRF (raw pXRF minus conventional Nb) and the Y/Nb ratio by conventional laboratory geochemistry, which illustrates the analytical interference argument: the more Y is present relative to Nb in a sample, the greater the Nb overestimation by pXRF. For basalts, Nb by pXRF still looks semi-quantitative; other unpublished data shows a better field performance for andesites and more felsic samples.

4. Discussion

4.1 Olympus Delta versus Vanta

The previous generation of pXRF analyzers from the same manufacturer was called the Olympus Delta Premium, and INRS tested two of those in previous work (Ross et al., 2014a, 2014b, 2016; Ross, 2019; Ross and Beaudette, 2021). It is interesting to compare the performance of the Delta Premium units (purchased in 2010) versus the Vanta series M units (purchased in 2020) on similar rocks to illustrate the technological evolution of these devices over a decade.

4.1.1 Sample precision

For *in situ* work on rock slabs and cut blocks, the minimum acceptable beam time was deemed to be 15-30 s on the Delta Premium, depending on the specific study (see references above), versus 10 s for the Vanta (this study). Since we were not using a specialized workstation in those previous studies with the Delta, but instead a laboratory stand, more time was needed to reposition the analyzer between spots to establish a firm contact with the sample. In bedrock mapping applications, we were therefore less demanding on the sample precision for some elements with the Delta, in order to keep the

total measurement time manageable, so we settled for a five-spot average for each sample (Ross, 2019; Ross and Beaudette, 2021). With the Vanta series M and use of a workstation, the shorter beam time and quick sample repositioning allows a nine-spot average, resulting in an improved sample precision for a similar total measurement time.

Table 4 compares the sample precision of the two generations of devices on similar (but not identical) porphyritic mafic volcanic samples from the Ungava Orogen, for both 5 point and 9 point averages, in both analytical modes. One way to use the table is to compare the Delta 5 point column with the Vanta 9 point column, since these data took us about the same time to acquire (10-12 mins per sample, both modes combined). This comparison shows significant improvement in RSD for most elements in favor of the Vanta, largely due to the increase in the number of spots for a similar total measurement time. However, some elements show an additional improvement in RSD for the same number of spots (e.g., Delta Mining Plus 9 points versus Vanta Geochem 9 points, or a similar comparison in Soil mode), which can be likely attributed to technological progress, most convincingly for CaO, P_2O_5 , SiO_2 , TiO_2 , Nb, and Sr. MgO is also much improved for the same number of spots, but is not directly comparable between the two samples due to very different concentrations, which are specifically higher in the sample tested with the Vanta. In summary, with the Vanta and the larger number of points, almost all of the RSDs are now below 10%, even in a strongly porphyritic mafic sample.

4.1.2 Accuracy and secondary calibrations

The secondary calibration exercise with the Vanta for *in situ* work on rocks shows that many elements exhibit a slope near one with y-intercepts close to zero on graphs of uncorrected pXRF versus conventional geochemistry (Figs. 6, 7; Table 3). This indicates that these elements have robust factory (primary/internal) calibrations, and don't need much secondary (external) calibration to provide accurate pXRF values, on average, based on the commissioning dataset. Examples shown on Figs. 6 and 7 include Al_2O_3 , CaO, K_2O , TiO_2 , Ni, Rb, Sr, Y and Zr, and other very well performing oxides based on the secondary calibration exercise are $Fe_2O_3^T$, MnO, and P_2O_5 (Table 3). The previous generation of pXRF analyzers from the same manufacturer needed more 'intense'

secondary calibrations for some of these same elements, in order to reduce the systematic errors (e.g., Ross et al., 2014a; Ross, 2019). Elements that still need notable secondary calibrations with the Vanta, even in the best performing analytical mode, include major oxides MgO and SiO₂, as well as trace elements Cr, Cu, Nb, V, and Zn (Table 3). So matrix-matched secondary calibrations are still needed, in general, to ensure accurate pXRF data.

The number of robust elements, i.e. those judged to generally give quantitative data after secondary calibration, is 19 with the Vanta, up from 16 with the Delta, using a similar methodology on similar Precambrian basement volcanic rocks (Ross, 2019 versus this study). The three extra elements that made the cut are Cu, P₂O₅ and V, although there are apparently still some analytical interferences with V and this element should be used with caution. Additional limitations with the Vanta are discussed below based on the validation exercise.

4.1.3 Validating the secondary calibration

Although the secondary calibration exercise showed very promising results for *in situ* pXRF measurements on rocks with the Vanta as summarized above, the real-life application, i.e. the bedrock mapping dataset, provides a more nuanced view. First, instrument drift over a period of months and years was detected for a few elements, notably SiO₂, and this needs to be carefully monitored in future studies by using several reference materials. Second, although we took care to select a very diverse range of igneous samples for the calibration exercise (from ultramafic to felsic and from tholeiitic to calc-alkaline), we still had to extrapolate the corrections beyond the calibrated range for several elements. Third, although precision and accuracy were satisfactory for most elements of interest for bedrock mapping, we had some unpleasant surprises for Al₂O₃ (poor precision, uncertain accuracy), Y (unexplained bias) and Nb (poor precision at low concentrations typical of basalts, plus significant analytical interference). So although the pXRF data is indeed robust for most elements of interest for bedrock mapping, pXRF will not replace conventional geochemistry over the short term.

4.1.4 Detection limits

We have not determined the detection limits in a statistically reliable way for *in situ* work on rocks for both instruments (Delta and Vanta), but we feel that the limits are probably lower on the Vanta for a number of elements. More work is required to demonstrate that claim quantitatively.

4.2 Using pXRF data in regional bedrock mapping projects

4.2.1 Using pXRF data in the field

Obtaining pXRF data in the field, a few days after the sample has been collected, allows geologists to compile a very preliminary geological map that also integrates insights from geophysical surveys, lithological and structural observations. This can be done partway through the mapping campaign and allows better planning of the rest of the field season. This might ultimately lead to a better end-result for the same number of field days, because attention can be put on mapping important areas such as contacts between geological formations. In the current study, we identified a marker horizon using pXRF data while in the field, and then traced it laterally. We also separated Mg-tholeiites from Fe-tholeiites and identified previously unrecognized formations. Furthermore, we used pXRF data to help with sample selection for U-Pb geochronology on zircons.

4.2.2 Drafting a preliminary geological map

A subset of samples analyzed by pXRF are also sent to a conventional geochemical laboratory, which might take a few months to report the results. Meanwhile, back in the office, geologists can use the pXRF data to produce a more refined preliminary geological map, of the type often seen in open house-type meetings. This preliminary map can separate visually similar units based on their geochemical signature even before the conventional geochemistry becomes available.

In our project, before the mapping began in 2021, volcanic rocks of the Roy Group in the study area were assumed to consist essentially of tholeiitic basalts from the Obatogamau and Bruneau formations. Using the pXRF data, we separated visually similar Fe-tholeiites from Mg-tholeiites into mappable units with the Obatogamau Formation and integrated

those on the preliminary map. We identified a marker horizon representing the top of the Obatogamau Formation based on its pXRF signature. This led to the rocks immediately above this marker horizon to be assigned to the felsic Waconichi Formation despite their metamorphic grade affecting preservation of primary textures. Further up the succession, the tholeiitic basalts were interpreted to be part of the Bruneau Formation, which is more continuous on the map than previously assumed. A layer of Mg-tholeiites was recognized at the base of the Bruneau Formation, like in the type locality further east. Finally, the Blondeau Formation was identified at the top of the succession.

4.2.3 Using pXRF data in the final geology map

For the final map and geological report, all of the geochemical data – conventional and pXRF – is typically available. So the final geochemical classification and grouping of volcanic rocks can be done using the higher precision, higher accuracy, more complete conventional geochemistry. However, once these groupings are defined or confirmed, pXRF can be used to interpolate between the conventional geochemical analyses on the final map, to get enough data points to produce chemo-stratigraphic polygons. This produces a more detailed map than would be available without pXRF data. In our case, the geochemical groupings from pXRF data generally held up, and the final geological map was very similar to the preliminary map. However, using corrected pXRF data and conventional laboratory data on the same geochemical diagram should be done only after the pXRF data has been validated one element at the time using conventional geochemistry.

5. Conclusions

Geochemistry is a very useful tool to map igneous rocks, but conventional laboratory geochemistry on new samples is not often available while in the field, and may not even be available quickly enough to prepare a preliminary geological map. Can portable X-ray fluorescence (pXRF) analyzers produce data of a suitable quality to distinguish between geochemically different groups of rocks for mapping purposes? To test this, we have utilized a pXRF analyzer *in situ* on rock slabs, in the context of a regional bedrock mapping project carried out by a government geological survey.

Even with the latest generation of pXRF analyzers such as the Olympus Vanta employed here, a commissioning step is required to determine the optimal analytical procedure for *in situ* measurements on rocks (measurement time and number of spots per sample), and to establish a matrix-matched secondary calibration. This step is also required to evaluate if the Geochem mode of the Vanta is sufficient on its own or if the Soil mode, based on a different algorithm, should also be employed. Here, based on studying 20 unmineralized Precambrian igneous samples ranging from komatiitic to rhyolitic and from tholeiitic to calc-alkaline, we determine that the following 19 oxides and elements are usable in bedrock mapping projects using a combination of the two analytical modes: Al_2O_3 , CaO , $\text{Fe}_2\text{O}_3^{\text{T}}$, K_2O , MgO , MnO , P_2O_5 , SiO_2 , TiO_2 , Cr , Cu , Nb , Ni , Rb , Sr , V , Y , Zn and Zr (although analytical interferences are suspected for V at low concentrations). Compared with the previous generation of instruments from the same manufacturer, the Vanta is faster for the same analytical precision, more accurate for many elements, usable on more elements, and we suspect that it has lower detection limits. To obtain the best sample precision in a reasonable time for routine samples, we opted to make 9 measurements on different spots per sample, but with a beam time of only 10 s, in both modes, representing about 10 minutes of pXRF measurements per sample. This is a larger number of spots, but faster time per spot, than that reported in previous studies, which were mostly using the previous generation of analyzers.

Once the pXRF device is commissioned, it can be used on routine samples during a regional bedrock mapping exercise (or many other applications). Here we have utilized it successfully on volcanic rocks, fine-grained to medium-grained intrusive rocks, and also sedimentary rocks derived from igneous sources, within the NE part of the Archean Abitibi Subprovince in Canada. The routine pXRF data, which becomes available a few days after each sample is collected, was first employed while still in the field. In particular, we used it along with all other available data to sketch a very preliminary geological map of the study area. Two visually similar types of tholeiitic basalts in the Roy Group, Mg-rich versus Fe-rich, were distinguished. We also identified a marker horizon which we then traced laterally during the last part of the field campaign.

Back in the office, before the conventional whole-rock geochemistry data became available, we prepared a much more detailed preliminary map, in time for presentation at an open house-type mining convention held in the fall. That preliminary map was substantially different from that available before our 2021 campaign, due in part to the abundant pXRF data on volcanic rocks. Specifically, the tholeiites of the Roy Group were assigned to two formations, Obatogamau and Bruneau, with the latter shown to be more continuous than previously thought. Both of these formations were separated into mappable units of Fe-tholeiite and Mg-tholeiite. In between the Obatogamau and the Bruneau formations, we identified a marker horizon of basalt with a transitional magmatic affinity at the top of the Obatogamau Formation, followed by the felsic and calc-alkaline Waconichi Formation. Finally, we showed that the intermediate to felsic Blondeau Formation occurs at the top of this succession, above the Bruneau Formation. These stratigraphic assignments, and the level of detail within the volcanic portion of the map, would not have been possible without the pXRF data.

Finally, the corrected pXRF data was also used during preparation of the final map, to interpolate between the conventional geochemistry samples. That final map was very similar to the preliminary one, unlike in mapping projects on Precambrian volcanic rocks for which no geochemistry of any kind is available for preparing the preliminary map.

Despite this successful demonstration of the advantages of having pXRF data for bedrock mapping projects, we do note some issues and limitations even with the latest generation of analyzers. Some analytical drift occurred between the calibration period and the mapping campaign (and also during the campaign) for some elements, such as Si, based on repeat measurements on a powdered reference material. We recommend using several reference materials with a range of concentrations to better monitor drift in future projects. Another unexpected issue was with Nb, which performed nicely during the calibration stage, but was then found to be commonly overestimated in the routine measurements, due mostly to analytical interferences with Y. Niobium is considered an important element for bedrock mapping because it occurs in a prominent volcanic rock classification diagram. For future work, we recommend to check whether longer beam

times or other strategies could improve the quality of Nb analyses by pXRF in basalts and other low-concentration rocks.

Declaration of interests

The authors declare that they have no known competing financial interests or personal relationships that could have appeared to influence the work reported in this paper.

Acknowledgements

This work was supported, financially and logistically, by *Ministère des Ressources naturelles et des Forêts du Québec*. Philippe Delobel acquired most of the pXRF data shown in figures 2-8 whereas summer students (Amélie Girard, Benjamin Leclerc, Laura Vachon) acquired the pXRF data shown in other figures. Francois Leclerc shared his geological expertise on the Chapais-Chibougamau region. Olivier Lamarche is acknowledged for discussions about analyzing Nb by pXRF. We thank two anonymous journal reviewers for constructive comments.

References

- Adams, C., Dentith, M., Fiorentini, M., 2021. Characterization of altered mafic and ultramafic rocks using portable XRF geochemistry and portable Vis-NIR spectrometry. *Geochemistry: Exploration, Environment, Analysis* 21, 1-21.
- Ahmed, A., Crawford, A.J., Leslie, C., Phillips, J., Wells, T., Garay, A., Hood, S.B., Cooke, D.R., 2020. Assessing copper fertility of intrusive rocks using field portable X-ray fluorescence (pXRF) data. *Geochemistry: Exploration, Environment, Analysis* 20, 81-97.
- Analytical Methods Committee, 2002. Fitting a linear functional relationship to data with error on both variables. AMC Technical Brief No. 10, 3 p.
- Barrett, T.J., MacLean, W.H., 1999. Volcanic sequences, lithochemistry, and hydrothermal alteration in some bimodal volcanic-associated massive sulfide systems, in: Barrie, C.T., Hannington, M.D. (Eds.), *Volcanic-associated massive sulfide deposits: processes and examples in modern and ancient settings*. Society of Economic Geologists, pp. 101-131.
- Beaudette, M., Bilodeau, C., Mathieu, G., 2020. Géologie de la région du lac Parent, Orogène de l'Ungava, Nunavik, Québec, Canada. Ministère de l'Énergie et des Ressources naturelles du Québec, report BG 2020-04.

- Beaudette, M., Ross, P.-S., Delobel, P., 2021. Analyseurs pXRF Vanta au MERN : optimisation des mesures et calibration pour le socle rocheux igné. Ministère de l'Énergie et des Ressources naturelles du Québec, report MB 2021-12, 54 p.
- Bezur, A., Lee, L., Loubser, M. Trentelman, K., 2020. Handheld XRF in cultural heritage – a practical workbook for conservators. Getty Conservation Institute, 191 p.
- Bourke, A., Ross, P.-S., 2016. Portable X-ray fluorescence measurements on exploration drill cores: comparing performance on unprepared cores and powders for “whole-rock” analysis. *Geochemistry: Exploration, Environment, Analysis* 16, 147-157.
- Conrey, R.M., Goodman-Elgar, M., Bettencourt, N, et al., 2014. Calibration of a portable X-ray fluorescence spectrometer in the analysis of archaeological samples using influence coefficients. *Geochemistry: Exploration, Environment, Analysis* 14, 291-301.
- Daigneault, R., Allard, G.O., 1990. Le Complexe du lac Doré et son environnement géologique, Ministère de l'Énergie, des Mines et des Ressources du Québec, report MM 89-03, 275 p.
- Daoudene, Y., Beaudette, M., 2021. Géologie de la région du lac La Trêve, Sous-province de l'Abitibi, Eeyou Istchee Baie-James, Québec, Canada. Ministère de l'Énergie et des Ressources naturelles du Québec, Québec Mines 2021, including a preliminary map at scale 1:50 000.
- Daoudene, Y., Beaudette, M., 2022. Géologie de la région du lac La Trêve, Sous-province d'Abitibi, Eeyou Istchee Baie-James, Québec, Canada. Ministère de l'Énergie et des Ressources naturelles du Québec, report BG 2022-04, including the final geological map at scale 1:50 000.
- Fisher, L., Gazley, M.F., Baenisch, A., Barnes, S.J., Cleverley, J., Duclaux, G., 2014. Resolution of geochemical and lithostratigraphic complexity: a workflow for application of portable X-ray fluorescence to mineral exploration. *Geochemistry: Exploration, Environment, Analysis* 14, 149-159.
- Frahm, E., 2017. First hands-on tests of an Olympus Vanta portable XRF analyzer to source Armenian obsidian artefacts. *IAOS Bulletin* 58, 8-23.
- Ge, L., Lai, W., Lin, Y., 2005. Influence of and correction for moisture in rocks, soils and sediments on in situ XRF analysis. *X-Ray Spectrometry* 34, 28-34.
- Hall, G.E.M., Buchar, A., Bonham-Carter, G., 2013. Quality control assessment of portable XRF analysers: development of standard operating procedures, performance on variable media and recommended uses; Phase I. Report for CAMIRO Project 10E01, 112 p.

- Hall, G.E.M., Bonham-Carter, G.F., Buchar, A., 2014. Evaluation of portable X-ray fluorescence (pXRF) in exploration and mining: Phase 1, control reference materials. *Geochemistry: Exploration, Environment, Analysis* 14, 99-123.
- Jensen, L.S., 1976. A new cation plot for classifying subalkalic volcanic rocks. Ontario Geological Survey, Miscellaneous Paper 66, 22 p.
- Jimenez-Gonzalez, J., 2020. Litho-geochemical analysis of the Heath Steele E Zone volcanogenic massive sulphide deposit, Bathurst mining camp, New Brunswick. MSc thesis, University of New Brunswick, 138 p.
- Leclerc, F., Bédard, J.H., Harris, L.B., McNicoll, V., Goulet, N., Roy, P., Houle, P., 2011. Tholeiitic to calc-alkaline cyclic volcanism in the Roy Group, Chibougamau area, Abitibi Greenstone Belt - revised stratigraphy and implications for VMS exploration. *Can. J. Earth. Sci.* 48, 661-694.
- Lemière, B., 2018. A review of pXRF (field portable X-ray fluorescence) applications for applied geochemistry. *J. Geochem. Explor.* 188, 350-363.
- Le Vaillant, M., Barnes, S.J., Fisher, L., Fiorentini, M.L., Caruso, S., 2014. Use and calibration of portable X-Ray fluorescence analysers: application to litho-geochemical exploration for komatiite-hosted nickel sulphide deposits. *Geochemistry: Exploration, Environment, Analysis* 14, 199-209.
- Lundblad S.P., Mills P.R., Drake-Rand A., Zikiloi S.K., 2011. Non-destructive EDXRF analyses of archaeological basalts. In: Shackley M. (eds) *X-Ray Fluorescence Spectrometry (XRF) in Geoarchaeology*. Springer, New York, p. 65-79.
- McNulty, B.A., Fox, N., Berry, R.F., Gemmill, J.B., 2018. Lithological discrimination of altered volcanic rocks based on systematic portable X-ray fluorescence analysis of drill core at the Myra Falls VMS deposit, Canada. *J. Geochem. Explor.* 193, 1-21.
- McNulty, B.A., Fox, N., Gemmill, J.B., 2020. Assessing hydrothermal alteration intensity in volcanic-hosted massive sulfide systems using portable X-ray fluorescence analysis of drill core: an example from Myra Falls, Canada. *Econ. Geol.* 115, 443-453.
- Martin, K.G., Carr, T.R., 2020. Developing a quantitative mudrock calibration for a handheld energy dispersive X-ray fluorescence spectrometer. *Sedimentary Geology* 398, article 105584.
- Olympus, 2021. Vanta family X-ray fluorescence analyzer – User’s manual, revision G (February 2021), downloaded from <https://www.olympus-ims.com/en/vanta/> on January 19, 2022.
- Piercey, S.J., Devine, M.C., 2014. Analysis of powdered reference materials and known samples with a benchtop, field portable X-ray fluorescence (pXRF) spectrometer: evaluation of

- performance and potential applications for exploration litho geochemistry. *Geochemistry: Exploration, Environment, Analysis* 14, 139-148.
- Potts, P.J., Webb, P.C., Williams-Thorpe, O., 1997. Investigation of a correction procedure for surface irregularity effects based on scatter peak intensities in the field analysis of geological and archaeological rock samples by portable X-ray fluorescence spectrometry. *Journal of Analytical Atomic Spectroscopy* 12, 769-776.
- Potts, P.J., Bernardini, F., Jones, M.C., Williams-Thorpe, O., Webb, P.C., 2006. Effects of weathering on in situ portable X-ray fluorescence analyses of geological outcrops: dolerite and rhyolite outcrops from the Preseli Mountains, South Wales. *X-Ray Spectrometry* 35, 8-18.
- Ripley, B.D., Thompson, M., 1987. Regression techniques for the detection of analytical bias. *Analyst* 112, 377-383.
- Ross, P.-S., 2019. Domaine Nord : protocole analytique pXRF pour utilisation pendant l'été 2019. Ministère de l'Énergie et des Ressources Naturelles, report MB 2019-04, 34 p.
- Ross, P.-S., Bédard, J.H., 2009. Magmatic affinity of modern and ancient subalkaline volcanic rocks determined from trace-element discriminant diagrams. *Can. J. Earth. Sci.* 46, 823-839.
- Ross, P.-S., Beaudette, M., 2021. Potentiel des analyseurs pXRF pour la cartographie régionale du socle rocheux au MERN : résultat d'un test dans le Domaine Nord de l'Orogène de l'Ungava. Ministère de l'Énergie et des Ressources naturelles du Québec, report MB 2021-05, 37 p.
- Ross, P.-S., Bourke, A., Fresia, B., 2014a. Improving lithological discrimination in exploration drill-cores using portable X-ray fluorescence measurements: (1) testing three Olympus Innov-X analyzers on unprepared cores. *Geochemistry: Exploration, Environment, Analysis* 14, 171-185.
- Ross, P.-S., Bourke, A., Fresia, B., 2014b. Improving lithological discrimination in exploration drill-cores using portable X-ray fluorescence measurements: (2) applications to the Zn-Cu Matagami mining camp, Canada. *Geochemistry: Exploration, Environment, Analysis* 14, 187-196.
- Ross, P.-S., Bourke, A., Mercier-Langevin, P., Lépine, S., Leclerc, F., Boulerice, A., 2016. High-resolution physical properties, geochemistry and alteration mineralogy for the host rocks of the Archean Lemoine auriferous VMS deposit, Canada. *Econ. Geol.* 111, 561-1574.

- Wells, T.J., Meffre, S., Cooke, D.R., Steadman, J., Hoye, J.L., 2021. Assessment of magmatic fertility using pXRF on altered rocks from the Ordovician Macquarie Arc, New South Wales. *Australian Journal of Earth Sciences* 68, 397-409.
- Wilke, D., Rauch, D., Rauch, P., 2016. Is non-destructive provenancing of pottery possible with just a few discriminative trace elements? *STAR: Science & Technology of Archaeological Research* 2, 141-158.
- Winchester, J.A., Floyd, P.A., 1977. Geochemical discrimination of different magma series and their differentiation products using immobile elements. *Chemical Geology* 20, 325-343.
- Zhang, W., Lentz, D.R., Charnley, B.E., 2017. Petrogeochemical assessment of rock units and identification of alteration/mineralization indicators using portable X-ray fluorescence measurements: Applications to the Fire Tower Zone (W-Mo-Bi) and the North Zone (Sn-Zn-In), Mount Pleasant deposit, New Brunswick, Canada. *J. Geochem. Explor.* 177, 61-72.

Figures

Fig. 1. Equipment setup and some sample photos (unpolished rock slabs). (a) Overview of the *Ministère des Ressources naturelles et des Forêts du Québec* (MRNFQ) field laboratory showing, from left to right, the rock density measurement station, the magnetic susceptibility station based on a KT-10 instrument (hidden from view), the pXRF station, the sample tracking board, and the sample photography station (mini studio). (b) Close-up view of the Vanta Workstation. (c) Interior of the Vanta Workstation showing the 12 mm grid and a typical rock slab. (d) Sample 19-GL-2141-A, the pyroxene (PX)- and plagioclase-phyric komatiitic basalt. (e) “Spinifex Ridge”, a komatiite sample with a random olivine spinifex texture. (f) Sample 2012-JG-9245-A, a plagioclase- and quartz-phyric rhyolite.

Fig. 2. Relative standard deviation (%) in the concentrations of Al_2O_3 , CaO, MgO, Sr, Y and Zr for a series of 30 spots spread over the sample, versus beam time (s), for sample 19-GL-2141-A (the porphyritic komatiitic basalt), in Geochem mode. The different curves in figures 2-5 represent moving averages for different numbers of spots: better

sample precision is achieved by averaging more spots, rather than by increasing beam time.

Fig. 3. Relative standard deviation (%) in the concentrations of K_2O , TiO_2 , Cu, Nb, Ni and Rb for a series of 30 spots spread over the sample, versus beam time (s), for sample 19-GL-2141-A (porphyritic komatiitic basalt), in Soil mode.

Fig. 4. Relative standard deviation (%) in the concentrations of Al_2O_3 , CaO, MgO, Sr, Y and Zr for a series of 30 spots spread over the sample, versus beam time (s), for sample “Spinifex Ridge” (spinifex-textured komatiite), in Geochem mode.

Fig. 5. Relative standard deviation (%) in the concentrations of Al_2O_3 , CaO, $Fe_2O_3^T$, Sr, Y and Zr for a series of 30 spots spread over the sample, versus beam time (s), for sample 2012-JG-9245-A (rhyolite), in Geochem mode. MgO is not shown here as it is below detection limit by pXRF in this sample.

Fig. 6. Conventional laboratory geochemistry (Agat Laboratory) versus uncorrected average of 30 pXRF spots per sample for Al_2O_3 (%), CaO (%), MgO (%), Sr (ppm), Y (ppm) and Zr (ppm), in Geochem mode, for the secondary calibration dataset. These elements and oxides are only available in Geochem mode, or perform better in this mode. For figures 6-8, the 20 samples from the calibration set are plotted ($n = 20$), except where indicated, with lesser numbers reflecting samples below the detection limit by pXRF and/or conventional geochemistry. Blue lines are linear regressions from Excel using all the displayed data; the pink line for MgO shows the higher slope for the first twelve samples. Short dashed lines have a slope of 1 and pass through the origin.

Fig. 7. Conventional laboratory geochemistry versus uncorrected average of 30 pXRF spots per sample for K_2O (%), TiO_2 (%), Cu (ppm), Nb (ppm), Ni (ppm) and Rb (ppm), in Soil mode, for the secondary calibration dataset. These elements and oxides perform better in this mode. All conventional laboratory data is from Agat Laboratory (back

squares and blue lines) except Nb also show from Activation Laboratories (green circles and green line).

Fig. 8. Conventional laboratory geochemistry versus uncorrected average of 30 pXRF spots per sample, for the secondary calibration dataset, for elements and oxides that perform better in the other mode (CaO, Cu, Nb; compare with Figs. 6-7), for elements that do not display robust behavior (As, Co), and for an element that can be calibrated but may show analytical interferences (V). All conventional laboratory data is from Agat Laboratory (back squares and blue lines) except Nb also show from Activation Laboratories (green circles and green line).

Fig. 9. Preliminary geological map of a portion of NTS sheets 32J04 and 32G13, showing geological contacts on an airborne geophysical background (first vertical derivative of the magnetic field), as well as pXRF data (bedrock mapping dataset) classified by geochemical groups, within the Roy Group volcanic rocks only. Originally drawn at a scale between 1:20 000 and 50 000 but reduced at a scale ~1:100 000 for the paper. Stratigraphic codes such as Ada, Alt, Pabi, etc. denote non-volcanic units, see Fig. 11 for details.

Fig. 10. Corrected portable XRF data (bedrock mapping dataset, average of 9 spots per sample), for the volcanic samples of the Roy Group only: (a)-(b) classification diagrams from Winchester and Floyd (1977); (c) magmatic affinity diagram from Barrett and MacLean (1999); (d) Jensen cation plot (Jensen, 1976), showing only basaltic samples. The corrected Nb values in (b) are based on the Agat Laboratory calibration (see Fig. 7), which was the only one available at the time that the geological mapping was being done. Even with the correction based on the second laboratory, Nb values are still overestimated in many samples, see text for discussion. Drift in SiO₂ not compensated in this figure. AB = alkali basalt. Tr/An = trachyandesite.

Fig. 11. Final geological map of the same area as shown in Fig. 9, showing the distribution of both pXRF and conventional geochemical data. Drawn at a scale between 1:20 000 and 50 000 but plotted at scale ~1:100 000.

Fig. 12. Corrected portable XRF data in Geochem mode (average of 9 spots per sample) versus conventional geochemistry for the bedrock mapping dataset: Al_2O_3 (%), $\text{Fe}_2\text{O}_3^{\text{T}}$ (%), MgO (%), SiO_2 (%), Y (ppm) and Zr (ppm). The correction for MgO is based on the 1-10% part of the calibration graph (first 12 points on Fig. 7), since the bulk of the bedrock mapping dataset is below 10% MgO and the fit between corrected pXRF and conventional geochemistry for the bedrock mapping dataset is better this way. For SiO_2 , 2.81 wt. % was added to the raw pXRF data, to account for instrument drift, before the correction was applied. The number of samples shown for different elements is variable due to analyses below the detection limit and a few gaps (missing information) in the pXRF data file. No outliers have been excluded except where noted.

Fig. 13. Corrected portable XRF data in Soil mode (average of 9 spots per sample) versus conventional geochemistry for the bedrock mapping dataset: K_2O (%), TiO_2 (%), Nb (ppm) and Rb (ppm). The corrections of pXRF data are based on the secondary calibrations (Agat Laboratory, see Fig. 7) except for Nb in the middle row of the right column (based on Activation Laboratories). No outliers have been excluded except one for Rb. The lower left panel shows the Nb overestimation (uncorrected pXRF minus conventional geochemistry) versus the Y/Nb ratio (conventional geochemistry) to demonstrate the interference of Y on Nb by pXRF in this dataset.

Author statement

We have not used AI during the writing of this paper.

Journal Pre-proof

Table 1. Traditional geochemistry (laboratory XRF) on the 20 igneous samples from the calibration set: major oxides*, wt. %, from Agat laboratory.

Sample	Rock type	Al ₂ O ₃	CaO	Fe ₂ O ₃ [†]	K ₂ O	MgO	MnO	P ₂ O ₅	SiO ₂	TiO ₂
Limit of detection		0.01	0.01	0.01	0.01	0.01	0.01	0.01	0.01	0.01
08-RR-6624	Tholeiitic rhyolite	8.9	0.1	1.9	1.9	0.8	0.05	0.01	82.0	0.10
08-RR-6627	Tholeiitic rhyolite	10.0	1.0	3.6	3.1	1.2	0.05	<0.01	78.0	0.11
2012-JG-9245-A	Calc-alkaline rhyolite	13.9	2.4	4.0	0.9	1.0	0.09	0.08	70.4	0.38
HWZ-010	Calc-alkaline rhyolite	13.1	0.5	6.6	1.9	1.1	0.23	0.07	70.9	0.36
MCL-12-09 (51.58 m)	Calc-alkaline felsic intrusion	16.5	2.5	1.4	2.6	0.5	0.02	0.04	68.2	0.14
130-PW-12	Tholeiitic dacite	10.4	0.2	5.6	0.2	10.2	0.03	0.12	67.7	0.66
DV-0009	Calc-alkaline dacite	14.3	4.4	6.8	1.2	3.8	0.12	0.14	62.2	0.98
MCL-12-09 (337.92 m)	Transitional andesite	14.7	5.2	8.6	0.1	5.0	0.19	0.09	55.5	0.74
2007-JG-5560-A	Calc-alkaline andesite	16.7	4.7	8.7	0.1	5.3	0.12	0.19	54.9	1.13
08-RR-6648	Tholeiitic basaltic andesite	13.8	6.6	8.6	0.1	7.2	0.15	0.11	57.3	1.05
19-SL-4051-A	Tr. to calc-alk. basaltic andesite	10.7	9.4	9.9	0.2	9.9	0.22	0.11	53.5	0.77
RO-469-A	Tholeiitic basalt	15.5	5.1	12.0	0.1	8.1	0.15	0.07	45.9	1.02
RO-470-A	Tholeiitic basalt	14.5	11.2	13.5	0.2	7.0	0.20	0.06	48.3	0.90
RO-471-A	Tholeiitic basalt	13.4	6.1	14.7	0.0	7.6	0.15	0.18	46.4	2.00
RO-476-A	Tholeiitic basalt	15.2	9.1	11.4	0.3	7.2	0.19	0.06	49.7	0.95
19-SM-6128-A	Tholeiitic to transitional basalt	15.2	8.1	15.4	0.1	7.6	0.23	0.29	44.9	1.95
19-GL-2141-A	Komatiitic basalt, porphyritic	11.7	11.6	11.6	0.9	14.2	0.17	0.10	44.6	0.87
RO-235	Komatiite	6.7	11.5	9.0	0.3	20.3	0.15	0.22	45.6	0.45
Spinifex Ridge	Komatiite	6.3	6.3	10.9	0.0	26.9	0.15	0.02	42.6	0.31
19-SL-4183-A	Peridotite (medium grained)	3.1	4.0	14.8	0.1	28.2	0.16	0.06	41.2	0.20

* Sodium, loss on ignition (LOI) and totals not reported here since these can't be measured with the pXRF, so they are not needed for the secondary calibration.

Table 2. Traditional geochemistry (ICP-OES and ICP-MS) on the 20 igneous samples from the calibration set: trace elements, ppm, from Agat laboratory except where noted.

Sample	Rock type*	As	Co	Cr	Cu	Nb [#]	Nb &	Ni	Rb	S	Sr	V	Y	Zn	Zr
Limit of detection		5	0.5	50	5	1	0.2	5	0.2	100	0.1	5	0.5	5	0.5
08-RR-6624	Tholeiitic rhyolite	LO D	0.7	205	58	23	18. 8	12	31. 5	300 0	23. 7	LO D	124	600 0	324
08-RR-6627	Tholeiitic rhyolite	LO D	0.5	137	LO D	26	22. 3	10	59. 8	LOD	36. 7	LO D	182	121	365
2012-JG-9245-A	Calc-alk. rhyolite	LO D	4.2	137	42	9	8.5	LOD	20. 1	180 0	118	24	34. 6	21	176
HWZ-010	Calc-alk. rhyolite	LO D	3.0	68.4	49	10	9.0	LOD	37. 0	560 0	18. 4	LO D	21. 4	321 0	174
MCL-12-09 (51.58 m)	Calc-alk. felsic intr.	LO D	2.8	LOD	LO D	LO D	0.7	5	58. 5	500	213	14. 0	2.0	37	62. 6
130-PW-12	Tholeiitic dacite	7	10. 7	68.4	45	20	15. 2	8	3. 3	LOD	5.1	19. 0	110	181	362
DV-0009	Calc-alkaline dacite	LO D	19. 6	137	19	8	7.9	5	26. 5	600	102	133	32. 6	205	188
MCL-12-09 (337.92 m)	Transit. andesite	LO D	28. 1	137	14	3	2. 2	5	1.0	160 0	192	167	17. 7	303	81. 6
2007-JG-5560-A	Calc-alk. andesite	13	30. 6	137	66	2	8.5	69	13. 2	150 0	173	191	31. 8	94	144
08-RR-6648	Thol. basaltic and.	LO D	42. 6	137	44	9	8.8	70	1.1	120 0	61. 2	283	65. 5	89	177
19-SL-4051-A	Tr. to c.-a. bas. and.	LO D	51. 1	137	63	5	5.1	306	4.0	120 0	137	177	16. 4	66	84. 3
RO-469-A	Tholeiitic basalt	8	45. 4	342	73	2	2.5	147	1.6	150 0	24. 5	269	17. 3	88	58. 3
RO-470-A	Tholeiitic basalt	LO D	45. 0	342	129	2	2.2	86	3.5	160 0	107	282	19. 9	87	50. 5
RO-471-A	Tholeiitic basalt	LO D	43. 7	137	63	6	6.5	54	0.8	800	55. 4	402	40. 1	98	138
RO-476-A	Tholeiitic basalt	LO D	49. 2	274	171	2	2.5	71	5.4	240	91. 1	304	20. 7	76	53. 3
19-SM-6128-A	Thol. tr. basalt	LO D	62. 2	274	102	10	10. 9	121	0.7	140 0	128	318	17. 5	110	77. 2
19-GL-2141-A	Komat. basalt	8	67. 9	130	96	2	1.9	282	19. 9	150 0	109	249	8.2	73	22. 9
RO-235	Komatiite	LO D	65. 7	212	23	2	1.8	657	6.1	260 0	164	115	9.0	63	50. 8
Spinifex Ridge	Komatiite	LO D	96. 0	239	35	LO D	0.4	133	0.4	150 0	31. 1	125	7.2	45	14. 2
19-SL-4183-A	Peridotite	LO D	105	616	28	LO D	0.7	442	0.7	120 0	75. 6	66	4.2	126	13. 8

* See table 1 for unabbreviated rock types.

[#] Nb from Agat Laboratory.[&] Nb from Activation Laboratories.

Table 3. Results of secondary calibration exercise on our pXRF Vanta device: linear regressions in both analytical modes.

Element/oxide	Mode	n*	m	b	R ²	Usable
Al ₂ O ₃ (%)	Geochem	20	0.9843	0.1063	0.9479	Yes
CaO (%)	Geochem	20	1.0123	0.1848	0.9917	Yes
CaO (%)	Soil	20	0.7716	0.3543	0.9788	Better in Geochem
Fe ₂ O ₃ ^t (%)	Geochem	20	0.9887	0.224	0.991	Yes
Fe ₂ O ₃ ^t (%)	Soil	20	0.6266	1.7558	0.9756	Better in Geochem
K ₂ O (%)	Geochem	13	0.9411	0.1169	0.9947	Better in Soil
K ₂ O (%)	Soil	19	1.0376	-0.0251	0.9721	Yes
MgO (%)	Geochem	16	0.7946	1.6692	0.9942	Yes
MnO (%)	Geochem	20	1.002	0.0098	0.9842	Yes
MnO (%)	Soil	20	0.9043	0.0143	0.9569	Better in Geochem
P ₂ O ₅ (%)	Geochem	17	1.0338	-0.0124	0.9239	Yes
P ₂ O ₅ (%)	Soil	17				No
SiO ₂ (%)	Geochem	20	0.8957	-0.6321	0.9729	Yes
TiO ₂ (%)	Geochem	20	1.1754	-0.0247	0.9742	Better in Soil
TiO ₂ (%)	Soil	20	1.0333	0.0587	0.987	Yes
As (ppm)	Both					No
Co (ppm)	Both					No
Cr (ppm)	Geochem	15	0.9537	90.365	0.9809	Better in Soil
Cr (ppm)	Soil	19	0.8668	78.517	0.9754	Yes
Cu (ppm)	Geochem	13	1.4313	-7.4013	0.8991	Better in Soil
Cu (ppm)	Soil	17	1.4225	2.5262	0.9422	Yes, maximum 175 ppm**
Nb (ppm) [#]	Geochem	9	1.122	2.4756	0.9935	Better in Soil
Nb (ppm) [#]	Soil	17	1.2725	-2.5755	0.9861	Yes
Nb (ppm) ^{&}	Soil	20	1.0471	-1.608	0.9620	Yes
Ni (ppm)	Geochem	17	0.9517	-1.8206	0.9958	Better in Soil
Ni (ppm)	Soil	19	1.0127	-2.0245	0.9969	Yes, maximum 1400 ppm**
Rb (ppm)	Geochem	17	0.9745	0.6319	0.9944	Better in Soil
Rb (ppm)	Soil	20	1.0325	-0.6542	0.9953	Yes
S (ppm)	Both					No
Sr (ppm)	Geochem	20	1.0025	1.6158	0.9819	Yes
Sr (ppm)	Soil	20	1.0657	-3.05	0.9847	Better in Geochem
V (ppm)	Geochem	14	1.2641	-50.678	0.9546	Yes, but possible interferences
V (ppm)	Soil	17				No
Y (ppm)	Geochem	19	0.9716	-0.7247	0.9972	Yes
Y (ppm)	Soil	20	1.1645	-2.756	0.9985	Better in Geochem
Zn (ppm)	Geochem	18	0.953	3.1433	0.9253	Yes, maximum 400 ppm**
Zn (ppm)	Soil	18	0.9064	8.4655	0.9126	Better in Geochem
Zr (ppm)	Geochem	20	0.9839	0.0032	0.9977	Yes
Zr (ppm)	Soil	20	1.1074	-1.4478	0.9965	Better in Geochem

* 'n' is the number of samples, out of 20, that could be used for the secondary calibration.

** The maximum concentrations for which our calibrations are valid for Cu, Ni and Zn are related to a lack of mineralized samples in the dataset.

[#] Based on conventional Nb from Agat Laboratory, like all other elements in this table.

& Based on conventional Nb from Activation Laboratories. See text for discussion.

Table 4. Sample precision (RSD in % of 30 measurements on different spots) of a Olympus Delta Premium device* versus a Olympus Vanta series M device** on similar porphyritic mafic volcanic samples from the Parent Group, Northern Domain of the Ungava Orogen.

Element / oxide	Delta, Mining Plus		Delta, Soil		Vanta, Geochem 3 beam		Vanta, Soil	
	5 pt ave	9 pt ave	5 pt ave	9 pt ave	5 pt ave	9 pt ave	5 pt ave	9 pt ave
Al ₂ O ₃	5.1	3.0	n.a.	n.a.	4.8	3.1	n.a.	n.a.
CaO	8.7	6.8	17	12	2.7	1.7	3.9	2.3
Fe ₂ O ₃	3.7	1.9	5.2	2.6	2.2	1.6	3.0	2.3
K ₂ O	15	9	17	13	19	14	18	13
MgO	14	11	n.a.	n.a.	2.6	1.9	n.a.	n.a.
MnO	4.2	1.2	6.3	3.0	1.9	1.3	2.7	2.0
P ₂ O ₅	LOD	LOD	LOD	LOD	14	8.7	LOD	LOD
SiO ₂	2.9	1.7	n.a.	n.a.	0.9	0.5	n.a.	n.a.
TiO ₂	6.1	5.4	10	8.1	4.9	3.5	4.9	3.5
Cr	15	8.2	50	38	15	8.7	16	9.0
Cu	13	7.5	14	11	23	11	24	14
Nb	n.a.	n.a.	LOD	LOD	LOD	LOD	10	9.1
Ni	7.1	5.7	LOD	LOD	4.0	3.1	4.4	3.4
Rb	n.a.	n.a.	21	15	15	11	16	11
Sr	n.a.	n.a.	20	13	3.2	5.6	7.8	4.6
V	8.3	5.4	7.2	5.4	7.5	4.4	3.3	1.9
Y	n.a.	n.a.	10	7.4	7.0	5.6	9.8	4.8
Zn	7.3	3.5	7.5	3.4	3.9	2.0	4.8	3.1
Zr	15	11	7.6	4.5	6.0	3.7	8.2	5.8

* Delta Premium device: 15 s per beam, 5 spot or 9 spot moving average, sample 18-SL-4165-A (traditional geochemistry: 13% CaO, 1.3% K₂O, 9% MgO, 44% SiO₂, 0.7% TiO₂, 280 ppm Cr, 116 ppm Cu, 75 ppm Ni, 20 ppm Rb, 381 ppm Sr, 8.7 ppm Y, 56 ppm Zn, 23 ppm Zr)

** Vanta device: 12 s per beam, 5 or 9 spot moving average, sample 19-GL-2141-A (traditional geochemistry: 12% CaO, 0.9% K₂O, 14% MgO, 44% SiO₂, 0.9% TiO₂, 300 ppm Cr, 96 ppm Cu, 282 ppm Ni, 20 ppm Rb, 109 ppm Sr, 8.2 ppm Y, 73 ppm Zn, 23 ppm Zr)

Abbreviations: n.a. = not available, LOD = device returns "LOD" (sample is below the limit of detection)

Highlights

- Portable X-ray fluorescence (pXRF) analyzers are very useful for bedrock mapping projects
- The pXRF data allows visually similar lithologies to be distinguished while in the field
- However a commissioning stage is required, and validation with conventional geochemistry

Journal Pre-proof

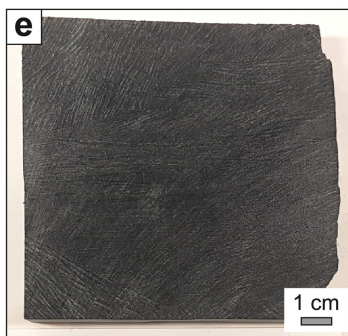
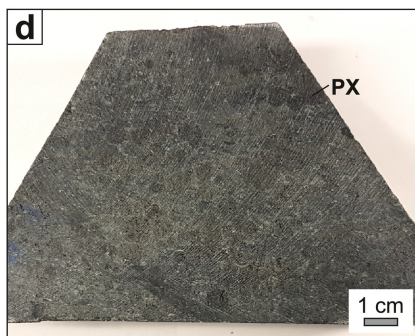


Figure 1

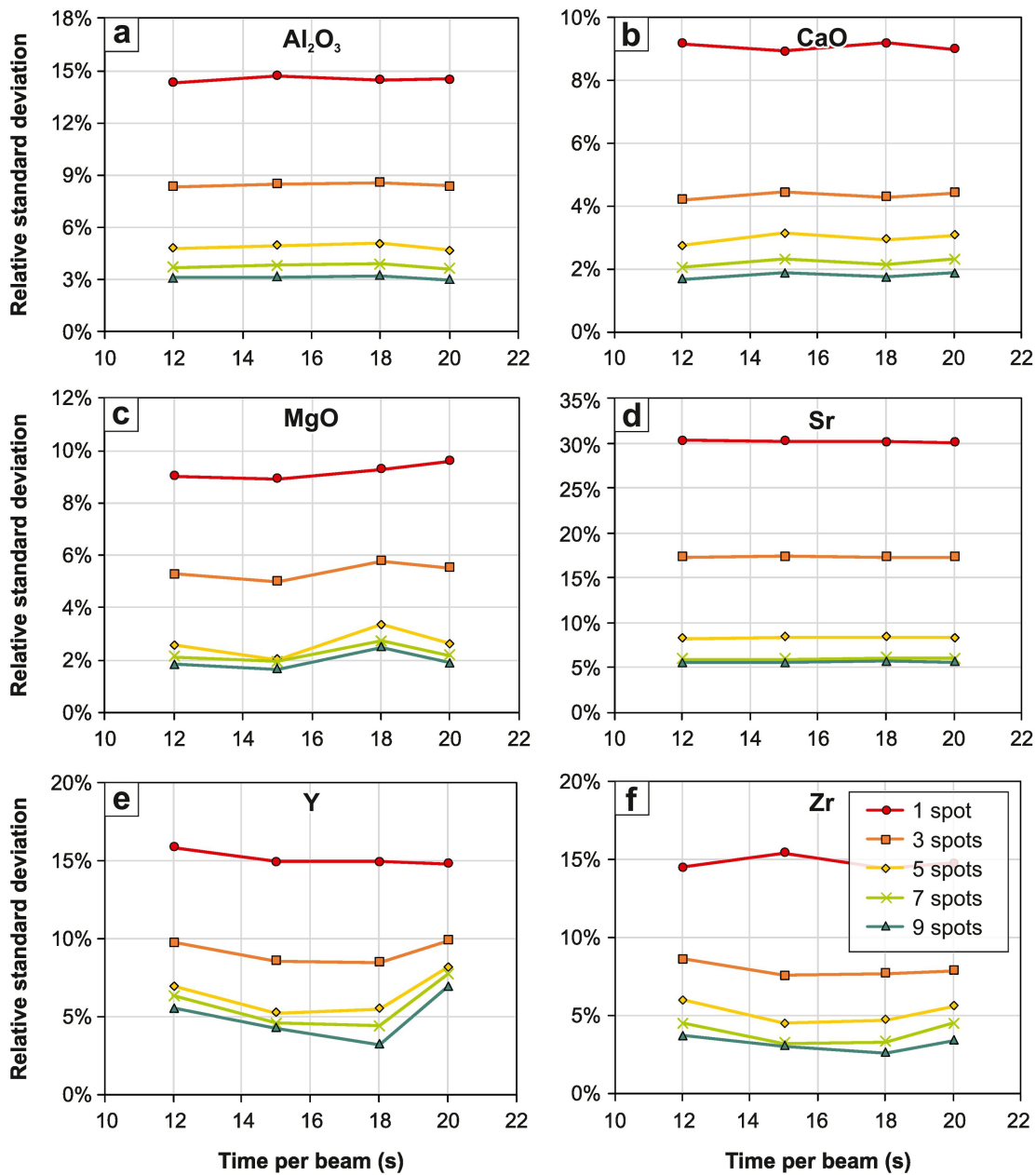


Figure 2

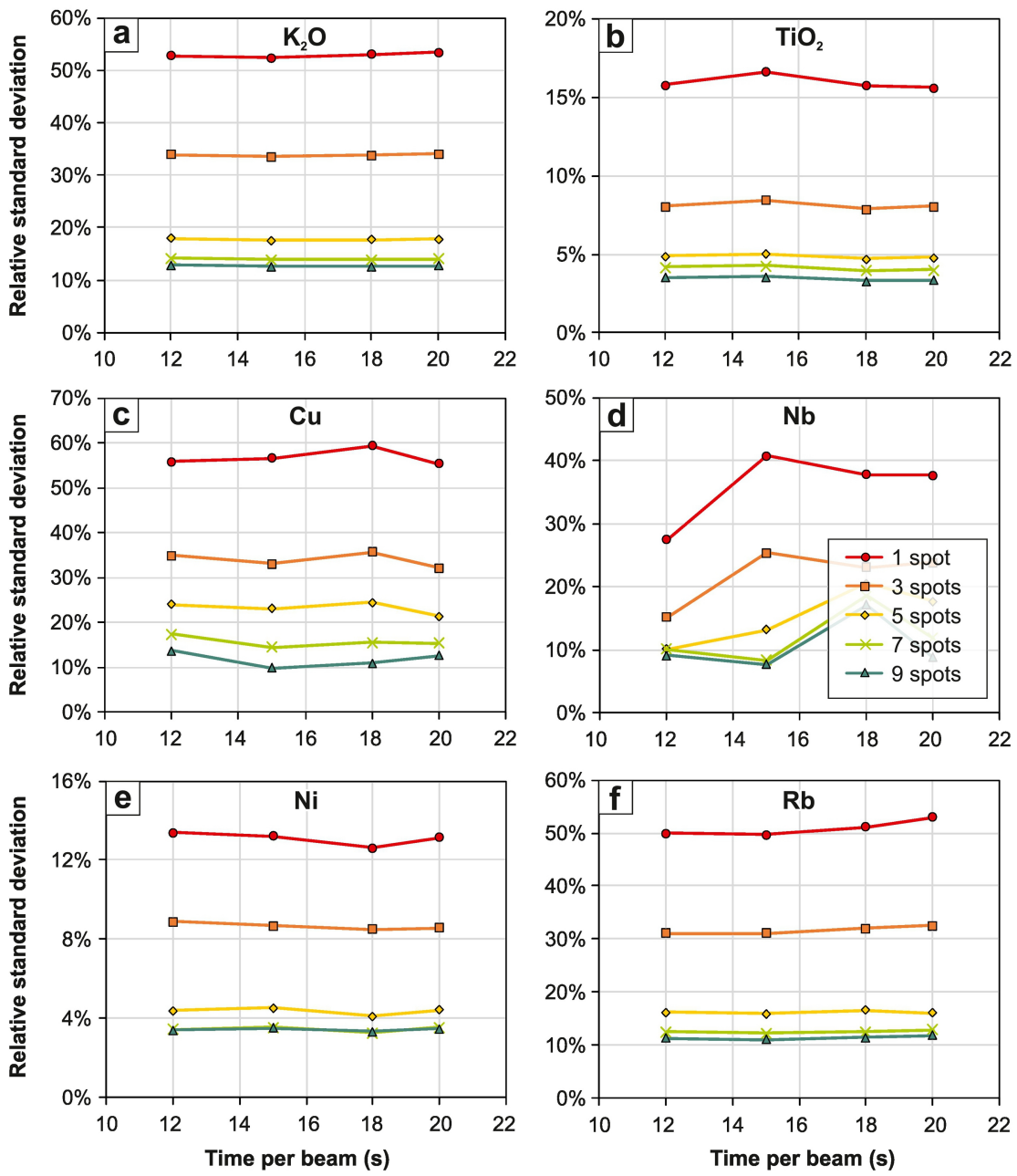


Figure 3

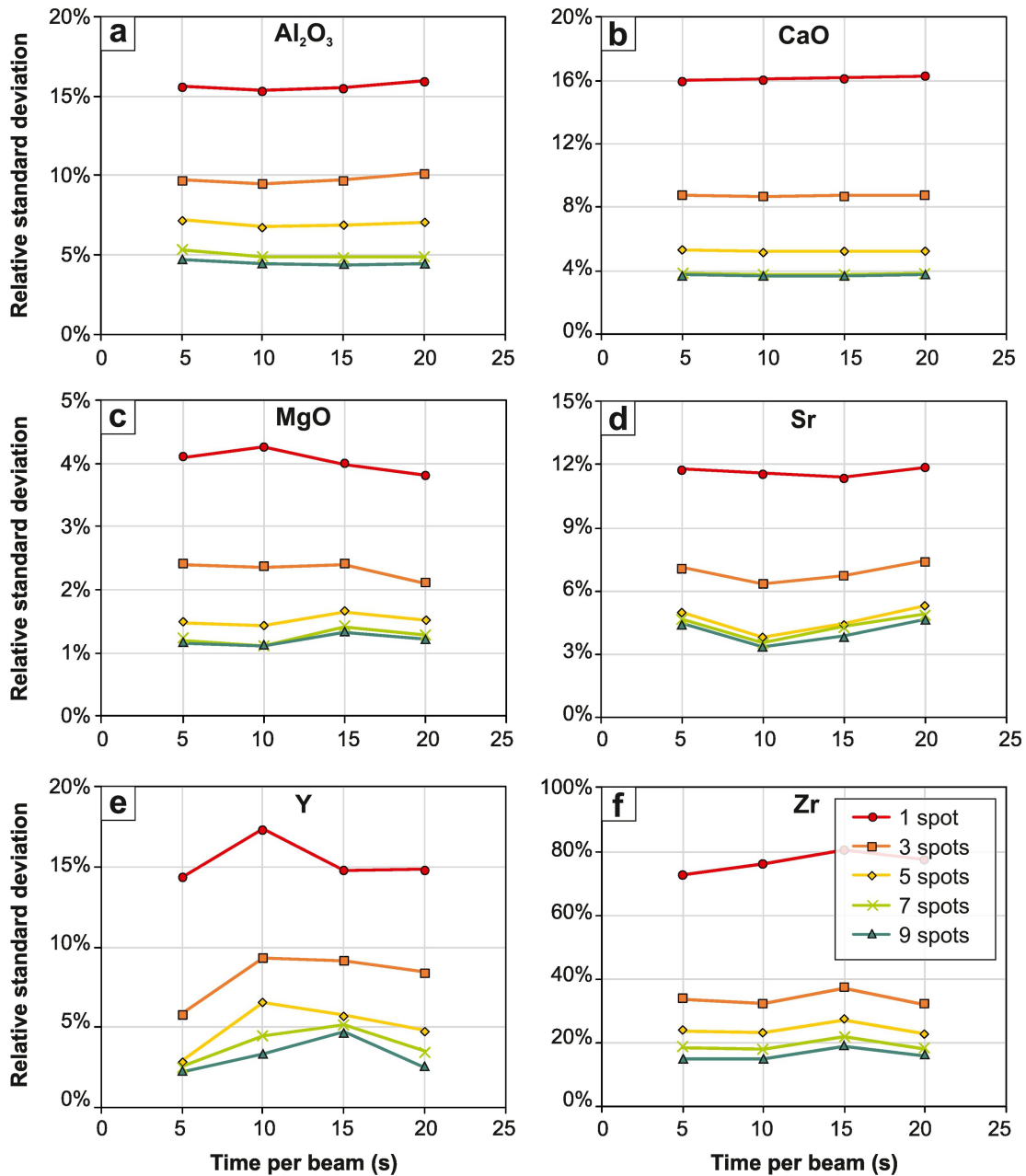


Figure 4

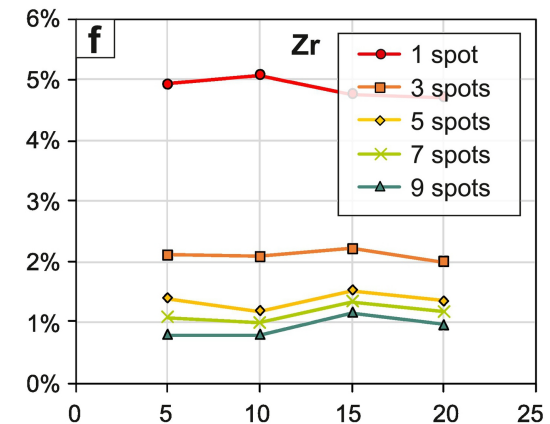
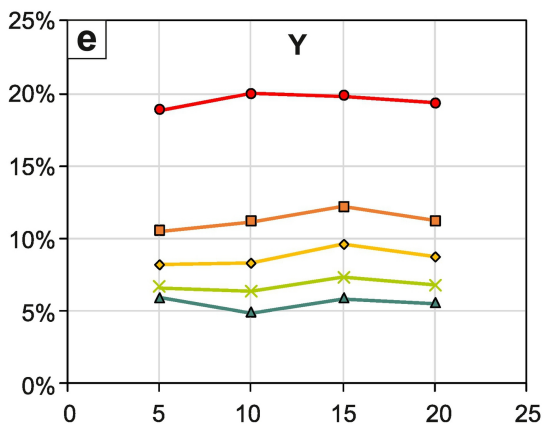
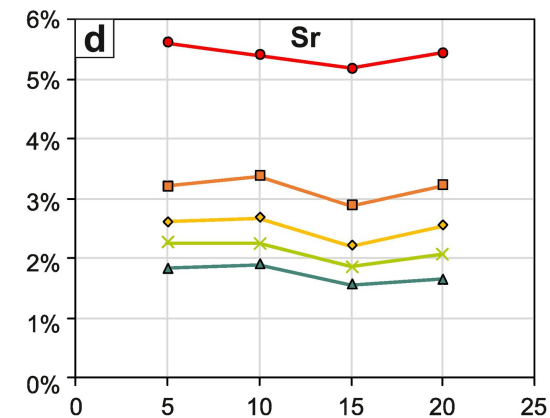
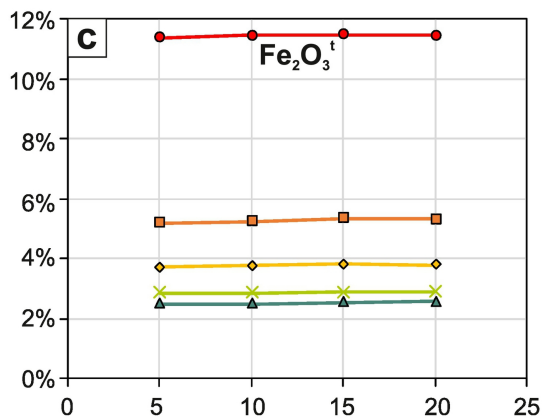
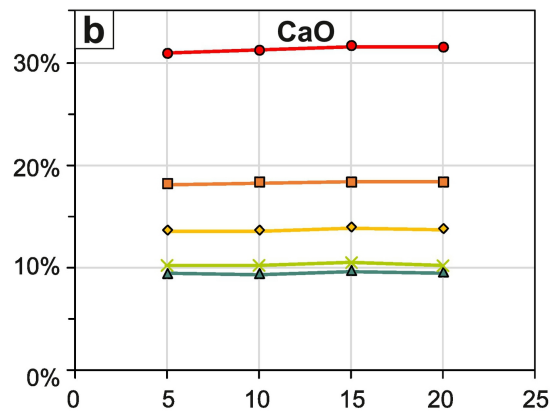
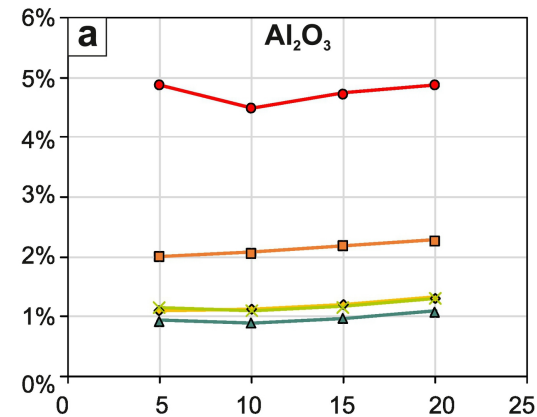


Figure 5

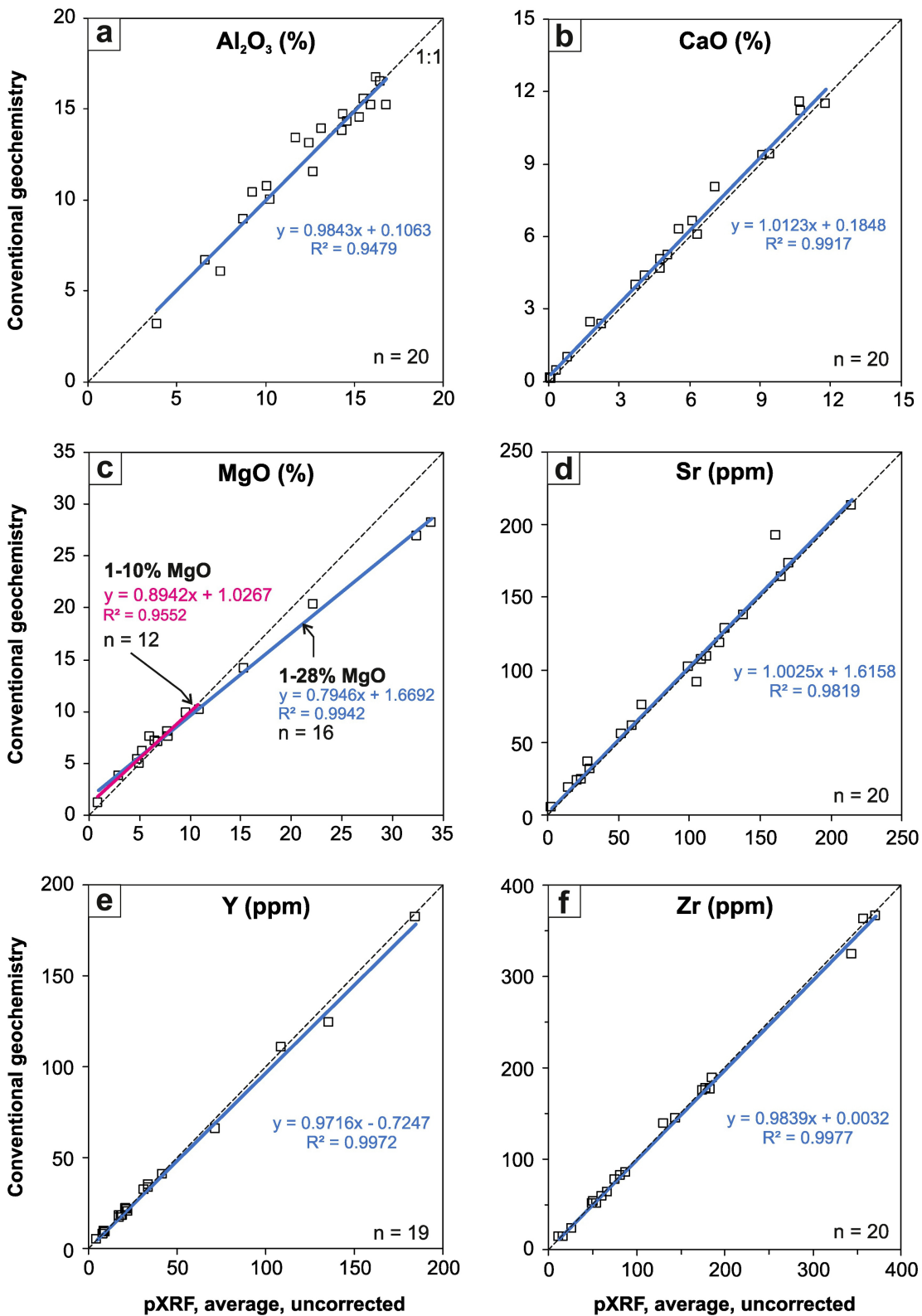


Figure 6

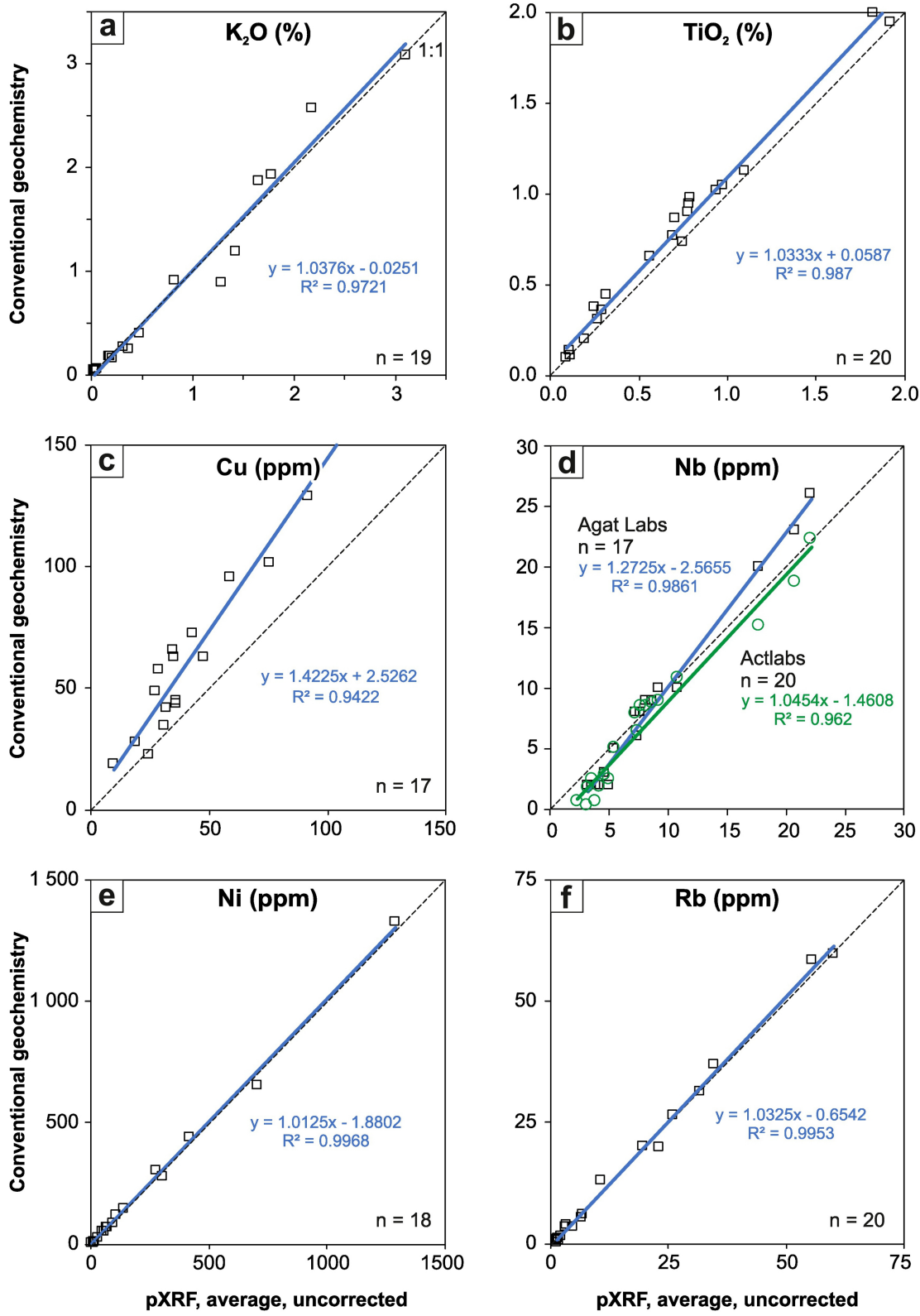


Figure 7

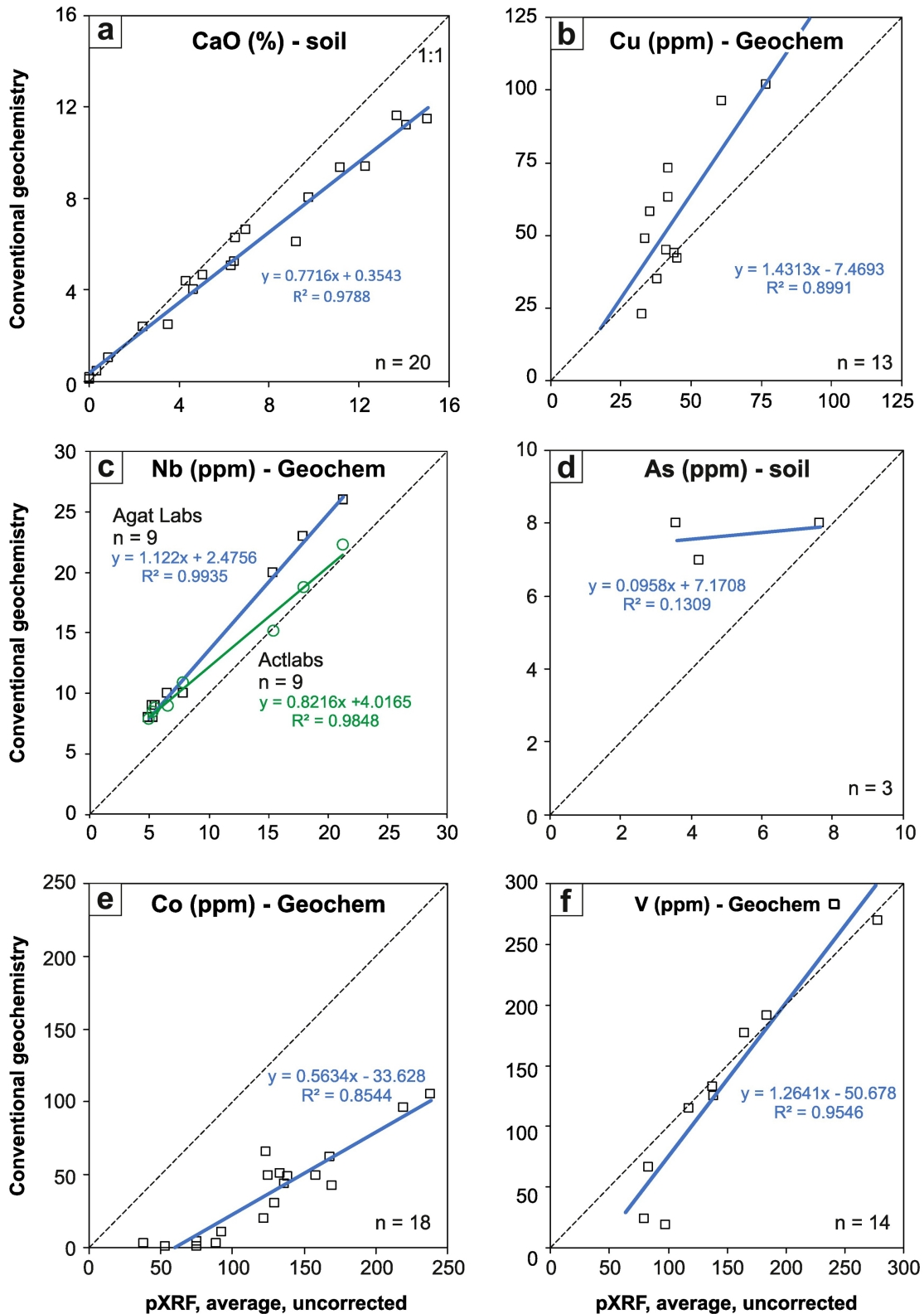


Figure 8

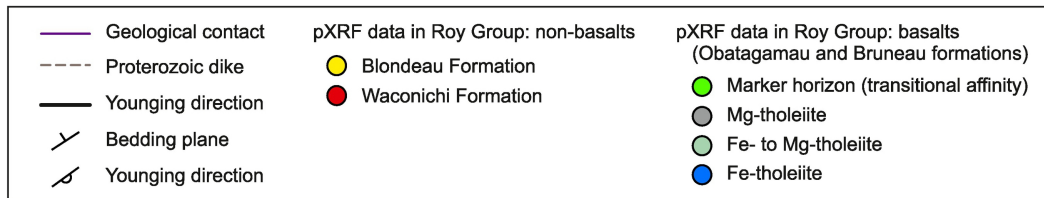
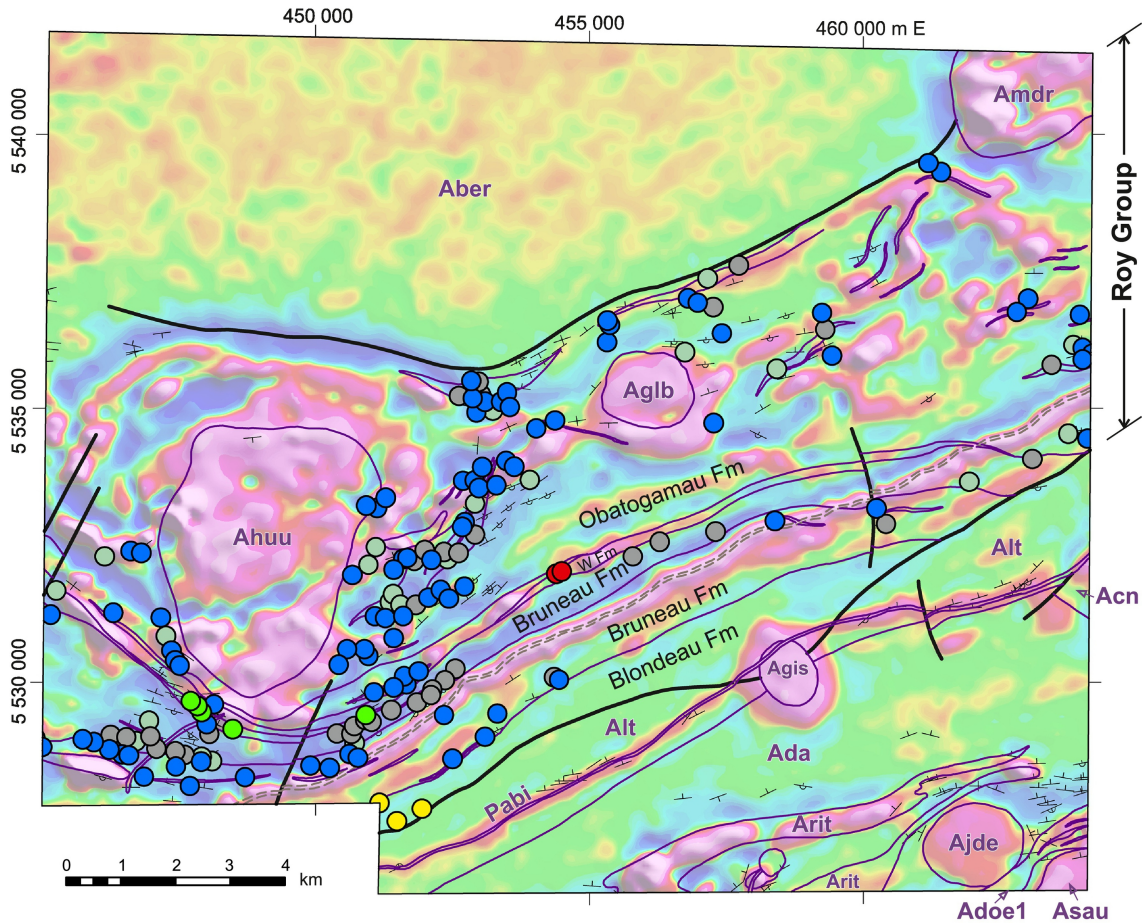


Figure 9

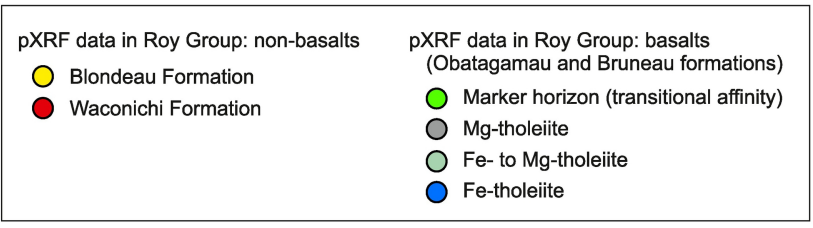
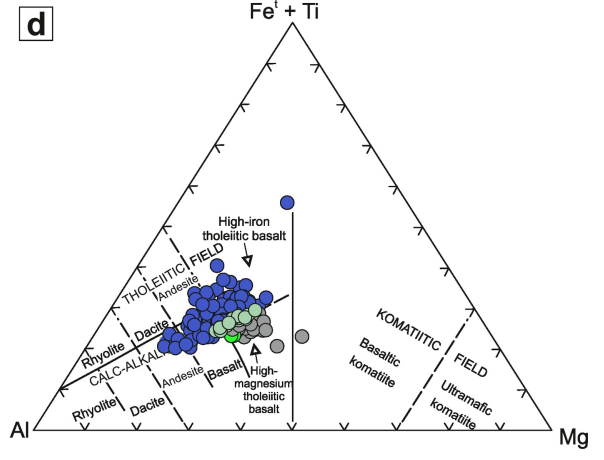
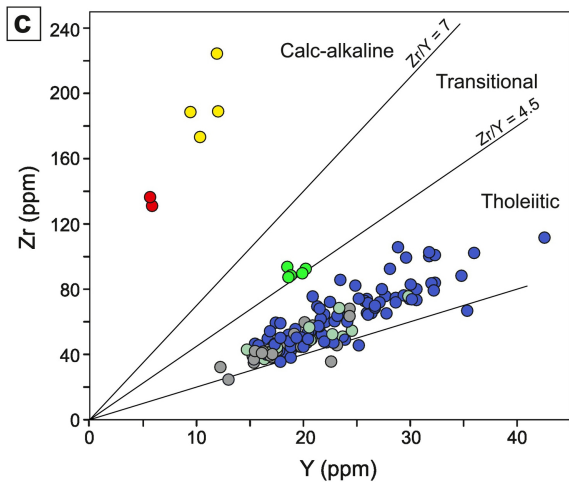
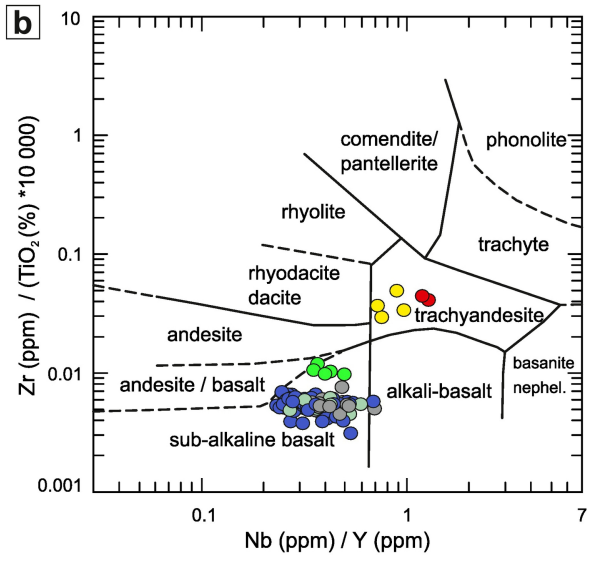
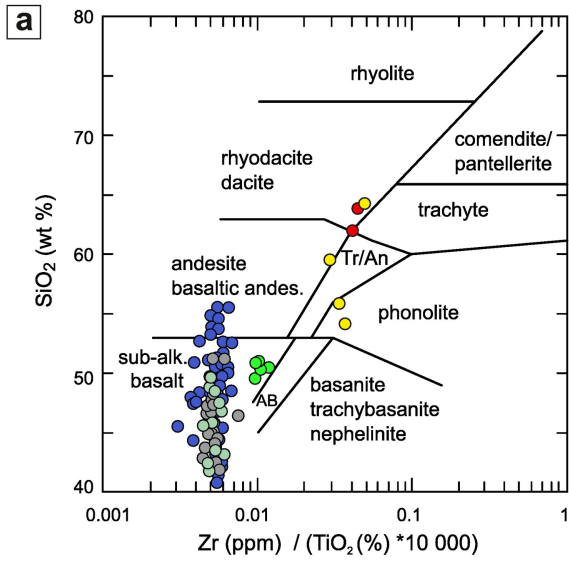


Figure 10

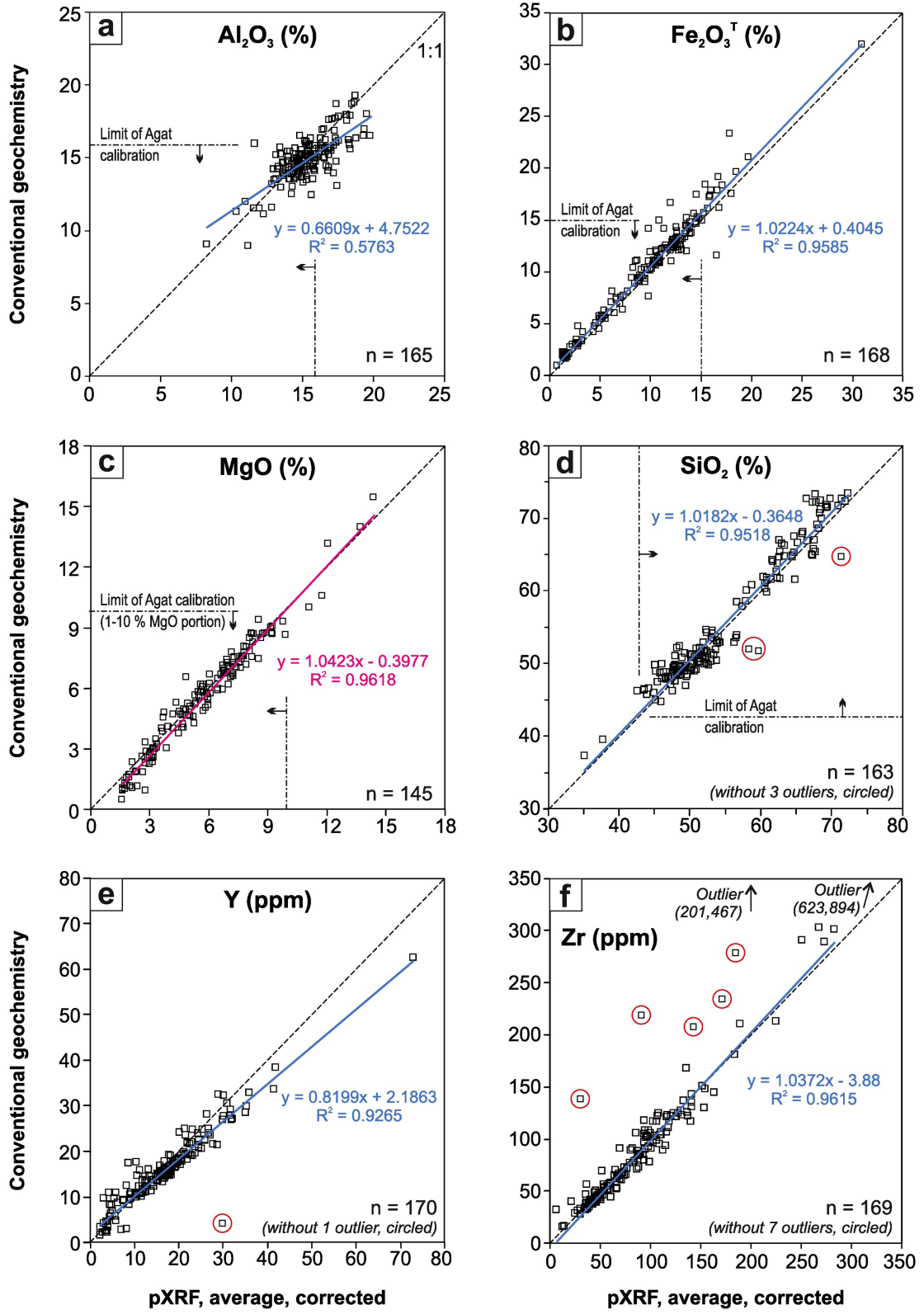


Figure 12

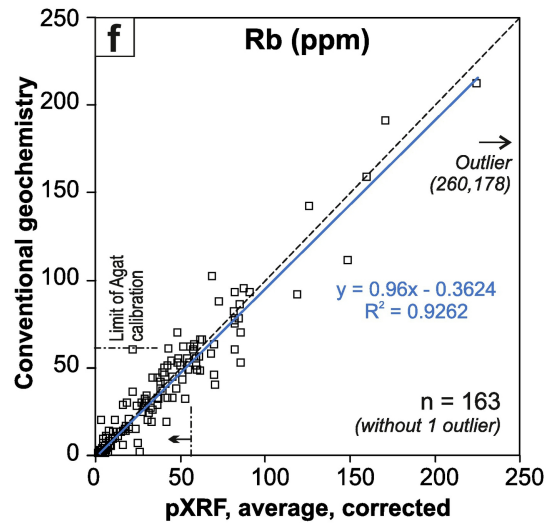
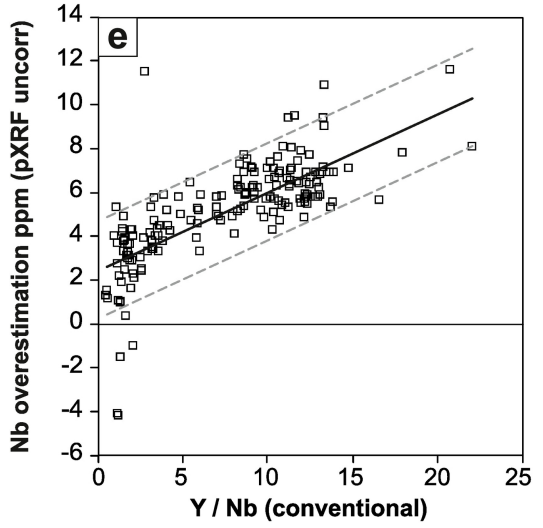
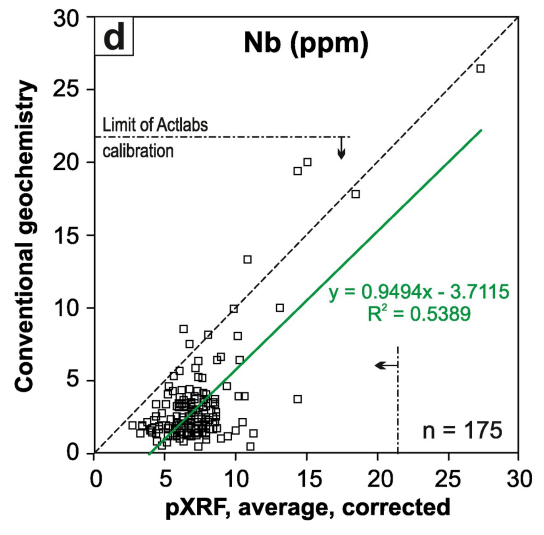
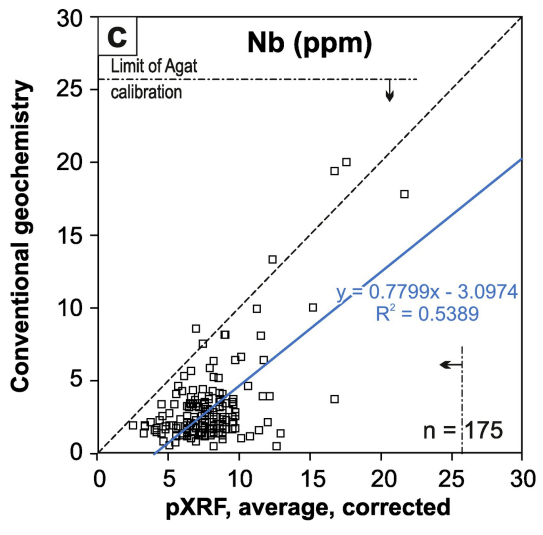
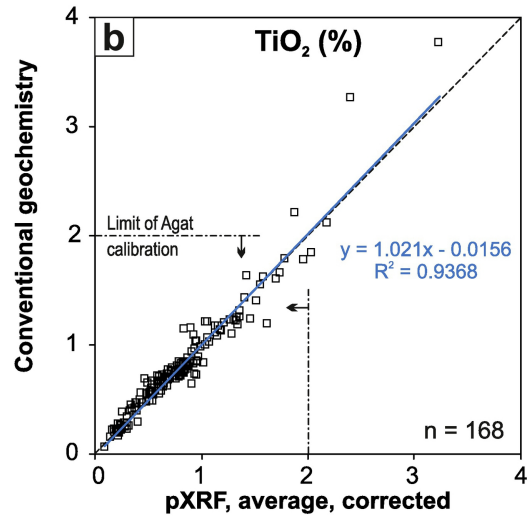
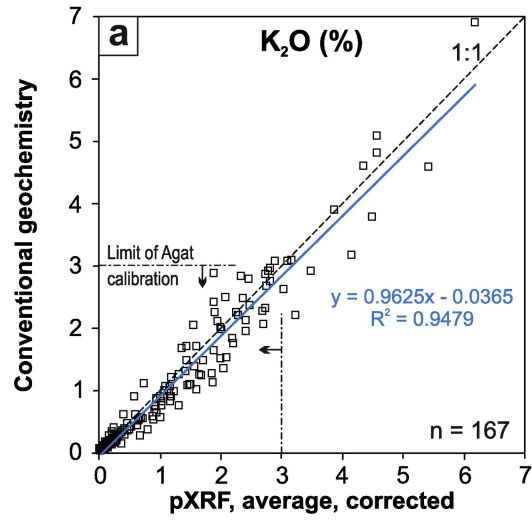


Figure 13